

Solcore: A multi-scale python-based library for the modelling of solar cells and semiconductor materials

D. Alonso-Alvarez^{a,*}, T. Wilson^a, P. Pearce^a, N. Ekins-Daukes^{a,b}

^a*Department of Physics, Imperial College London, London, United Kingdom*

^b*School of Photovoltaic and Renewable Energy Engineering, University of New South Wales, Sydney, Australia*

Abstract

Solcore was born as a modular set of tools, written entirely in Python 3, to address some of the task we had to solve more often, such as fitting dark IV curves or luminescence decays. With time, however, it has evolved as a complete semiconductor solver able of modelling the optical and electrical properties of a wide range of solar cells, from quantum well devices to multi-junction solar cells. At present, it is a multi-scale simulation framework, with applicability from the nanoscale and the quantum properties of semiconductors nanostructures to assessing the performance of solar arrays or the modelling of the spectral irradiance based on atmospheric conditions. In this article we summarize its main characteristics as well as the physical insight and mathematical formulation behind the software with the purpose of serving both as a research and teaching tool.

Keywords: solar cells modelling; quantum solvers; semiconductor properties; solar irradiance; optical modelling.

1. Introduction

Modelling and simulations are at the heart of modern research in solar energy, either to understand the absorption of sunlight by different materials, to optimize a solar cell structure to maximize performance, or to predict the annual energy yield of a technology in a given geographical location, among many others. Along the years, and with different degrees of sophistication, many pieces of software have been developed and published to tackle different aspects of solar energy research. For example, to calculate the solar spectrum as a function of the atmospheric conditions a traditional solution is using SMARTS [1]; the light absorption profile in the solar cell or even at module level could be addressed by OPTOS [2] or OPAL2 [3]; while to solve the transport equations of a solar cell one could use PC1D or Quokka [4]. Several free and commercial programs, not specifically designed for solar energy research, have also been historically used such as AFORS-HET [5], Nextnano [6] or Atlas [7], the first two focused on the device and semiconductor properties and the later also solving the optics of the solar cells. An extensive list of software for solar energy research - both online calculators and downloadable programs - have been compiled by PV Lighthouse.

Except for a few exceptions, such as PVlib [8], all these solvers are high level, self-contained applications. While users can provide their own inputs and, in some cases, access the source code of the programs and customize some aspects of them, they are not designed with that purpose in mind.

Solcore is a multiscale, modular simulation framework for solar energy research, written mostly in Python with the ex-

plicit purpose of simplifying its integration in other programs, its expansion with custom routines and algorithms, and of being didactic and informative. It is a teaching and learning tool as much as a rigorous research tool, being the most recent version released under the GNU Lesser General Public License (GNU-LGPL).

Solcore's capabilities can be grouped into four categories: materials science (Section 2), light sources (Section 3), solar cells (Sections 4 to 6) and large scale calculators (Section 7), each of them tackling a different area - and scale - related to the research in solar energy. Figure 1 shows how these parts relate to each other as well as summarizing some of their content.

2. Materials science

The materials science modules in Solcore deal with the retrieval and calculation of material properties as well as those of quantum nanostructures, in particular quantum wells. They form the building blocks necessary to create the structures and calculate the performance of full solar cell devices. While focused on its application for solar cells, this part of Solcore is widely applicable to any research area related to semiconductor materials, as a way of managing the material properties, customising them and using them in other calculations.

2.1. Parameters database

The parameters database contains the basic properties of many semiconductor materials, including silicon, germanium and many III-V semiconductor binary and ternary alloys. Among other parameters, it includes the energy bandgap, the electrons and holes effective masses, the lattice constants or the elastic constants.

*Corresponding author.

E-mail address: d.alonso-alvarez@imperial.ac.uk

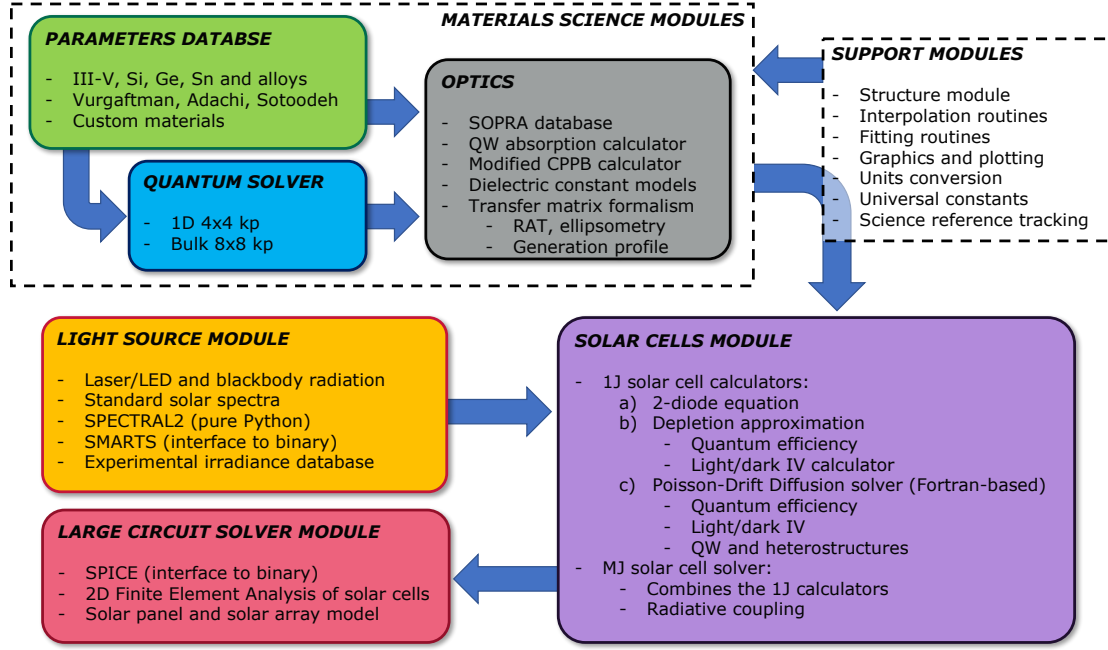


Figure 1: General structure and workflow of Solcore [UPDATE with Optics module and correct electrical solvers]

The main sources of data are the article by I. Vurgaftman on *Band parameters for III-V semiconductors*[9] and the *Handbook Series on Semiconductor Parameters* by Levinshstein et al. [10]. The carrier mobility calculator is based on the empirical low-field mobility model by Sotoodeh et al. [11] and it is available only for some materials where the inputs for the model are available.

There are two methods for retrieving parameters from the database. The first one consists simply of getting the data using the `get_parameter` function with the required inputs. For example:

```
get_parameter("GaAsP", "band_gap", P=0.45, T=300)
```

will return the bandgap of GaAsP for a phosphorus concentration of 45% at a temperature of 300 K, equal to 1.988 eV. This method only uses the existing data. Another method is to create a material object which will contain all the properties existing in the database for that material, as well as those included as input, which will override the value of the database parameter, if it exists. The following example creates a GaAs object and an AlGaAs object, using a custom electron effective mass in the latter:

```
GaAs = material("GaAs")(T=300, Na=1e24)
AlGaAs = material("AlGaAs")(T=300, Al=0.3, Nd=1e23, eff_mass_electron=0.1)
```

Now, any parameter - including the custom ones - are attributes that can be easily accessed and used anywhere in the program. For example `GaAs.band_gap` is the GaAs bandgap and `AlGaAs.lattice_constant` is the AlGaAs lattice constant, both at the composition and temperature chosen when creating the objects.

Figure 2 shows the well known bandgap vs. lattice constant map of all semiconductor materials and alloys (only ternary

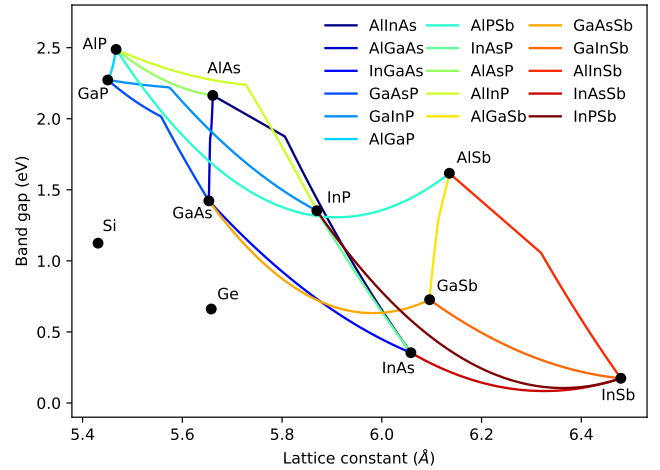


Figure 2: Materials with most parameters included in the Solcore's database (excluding the optical properties).

compounds) currently implemented into Solcore. However, any other material can be used in all of the Solcore functions, as long as the needed input parameters are provided. This can be done by overriding all the properties of an existing material during the creation as above, or adding it as an external material in the configuration files.

2.2. Optical Properties Database

In order to calculate and model the optical response of potential solar cell architectures and material systems, access to a library of accurate optical constant data is essential. Therefore, Solcore incorporates a resource of freely available optical constant data measured by Sopra S. A. and provided by Software

Spectra Inc. [12]. The refractive index n and extinction coefficient k are provided for over 200 materials, including many III-V, II-VI and group IV compounds in addition to a range of common metals, glasses and dielectrics.

Any material within the Sopra S. A. optical constant database can be used with the "material" function described above, but they will have only the optical parameters n and k . In the case of materials that are in both databases, the keyword "sopra" will need to be set to "True" when creating the material. Once a material is loaded its n , k and absorption coefficient data is returned by calling the appropriate method, for example `SiO2.n(wavelength)` and `SiO2.k(wavelength)`. For certain materials in the database, the optical constants are provided for a range of alloy compositions. In these cases, any desired composition within the range can be specified and the interpolated n and k data is returned. Several examples about creating materials from the Sopra database are shown in the Listing 1.

```
# Normal GaAs material with all the parameters
GaAs = material("GaAs")()

# Sopra version, with only optical constants
GaAs_sopra = material("GaAs", sopra=True)()

# Ni, Au and SiO2 are only in the Sopra database,
# so there is no need to include a flag
Ni = material("Ni")()
Au = material("Au")()
SiO2 = material("SiO2")()

# Creating materials with different alloy
# compositions
AlGaAs_sopra = material("AlGaAs", sopra=True)(Al
=0.4)
HgCdTe = material("HgCdTe")(Cd=0.25)

# Relaxed SiGe alloys
SiGe25 = material("ReSiGe")(Si=0.25)
SiGe75 = material("ReSiGe")(Si=0.75)
```

Listing 1: Creating Solcore materials from the Sopra database.

Figure 3 highlights example output from the Sopra materials library with 3a showing GaAs and Ge optical constant data and 3b showing interpolated AlGaAs extinction coefficients for a range of aluminium fractions.

2.3. Quantum solver

The electronic band structure of semiconductor materials is responsible for their light absorption and emission properties as well as for many of their transport properties, ultimately depending on the carriers effective masses. These properties are

not intrinsic of the material, but depend on external factors, too, most notably the strain and the quantum confinement.

Given the crystalline nature of most semiconductor materials, strain is a factor often present, whenever two materials with different crystal lattice constants are grown on top of each other pseudomorphically. Even those with the same lattice constant might be under stress due to other effects such as the presence of impurities or if used at different temperatures having dissimilar thermal expansion coefficients. Quantum confinement, in turn, takes place when the size of the semiconductor material in one or more dimensions is reduced to a few nanometres. In that situation, the energy levels available to the carriers become quantized in the direction of confinement, also changing the density of states. Both conditions take place simultaneously when dealing with strain balanced quantum wells (QW).

Quantum wells - and more recently quantum wires - have been employed to tune the absorption properties of high efficiency solar cells for the past two decades. The need for appropriate tools to study them in the context of photovoltaics led to the development of the simulation models that were the seed of Solcore [13, 14, 15, 16]. As strained materials with quantum confinement, special care must be taken to obtain a sensible set of parameters for the QW structures, including the band edges with confined energy levels, the effective masses and the absorption coefficient.

Solcore's approach for evaluating the properties of QWs involves calculating first the effect of strain using a 8-bands Pikus-Bir hamiltonian (Section 2.3.1), treating each material in the structure as bulk, and then using the shifted bands and effective masses to solve the 1D Schödinger equation, after a proper alignment between layers (Section 2.3.2) [17]. Finally, the absorption coefficient is calculated based on the 2D density of states, including the effect of excitons (Section 2.5).

2.3.1. Bulk 8-band $\mathbf{k} \cdot \mathbf{p}$ calculator

There are many numerical methods to calculate the band structure of a material with a varied degree of sophistication and complexity, such as the tight binding, the pseudopotential, the Green's function or the $\mathbf{k} \cdot \mathbf{p}$ method. Solcore includes a modified 8-band Pikus-Bir hamiltonian to calculate the band structure of bulk materials under biaxial strain [18], considering the coupling between the conduction, heavy hole, light hole and split-off bands. The eigenfunctions Ψ and eigenstates E are the solutions of the following equation, with \mathcal{H} is the Pikus-Bir hamiltonian:

$$\mathcal{H}\Psi = \begin{pmatrix} E_{cb} & -\sqrt{3}T & \sqrt{2}U & -U & 0 & 0 & -T^* & -\sqrt{2}T^* \\ & E_{hh} & \sqrt{2}S & -S & 0 & 0 & -R & -\sqrt{2}R \\ & & E_{lh} & -\sqrt{2}Q & T^* & R & 0 & \sqrt{3}S \\ & & & E_{so} & \sqrt{2}T^* & \sqrt{2}R & -\sqrt{3}S & 0 \\ & & & & E_{cb} & -\sqrt{3}T^* & \sqrt{2}U & -U \\ & & & & & E_{hh} & \sqrt{2}S^* & -S^* \\ & & & & & & E_{lh} & -\sqrt{2}Q \\ & & & & & & & E_{so} \end{pmatrix} \Psi = E\Psi$$

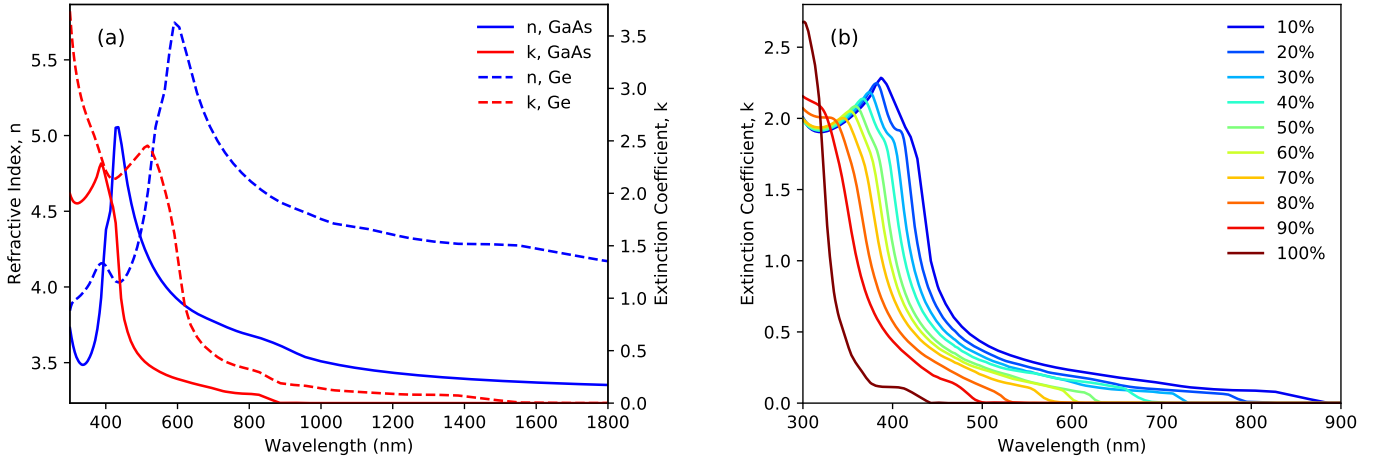


Figure 3: Example output from the Sopra S. A. optical constant database accessed from Solcore. (a) Refractive index and extinction coefficient data for GaAs (solid lines) and Ge (dashed lines). (b) Interpolated AlGaAs extinction coefficient data with aluminium fractions ranging from 10 to 100%.

Here, the sub-diagonal elements are just the complex-conjugate of the corresponding elements upper ones. Diagonal terms have three components: the information about the unstrained band edges, a kinematic term and a strain term. As an example, the term E_{cb} is given by:

$$E_{cb} = E_{c0} + O_k + O_\epsilon \quad (1)$$

$$O_k = \frac{\hbar^2}{2m_0} \gamma_c (k_x^2 + k_y^2 + k_z^2) \quad (2)$$

$$O_\epsilon = a_c (\epsilon_{xx} + \epsilon_{yy} + \epsilon_{zz}) \quad (3)$$

where E_{c0} is the position of the unstrained conduction band edge, γ_c a modified Luttinger parameter, the k_i the momentum in the different directions of the reciprocal space, a_c the conduction band hydrostatic deformation potential and the ϵ_{ij} s the strain tensor components. Off-diagonal term have similar expressions, just not involving the unstrained band edges. A detailed description of all these terms and their origin can be found in Tomic [18].

This system is readily solved for the given k_i using Numpy's `linalg.eig` function, which provides as output the eigenfunctions and the corresponding eigenvalues. Typically, we are interested in the new band edges due to the effect of strain and the resulting effective masses, given by the curvature of the bands near $k_i = 0$. Fig. 4 shows an example of the bands calculated in this way for the case of a strained InGaAs layer grown pseudomorphically on GaAs, and the resulting dependence of the effective mass with the indium content of the layer. Notice that, due to the effect of strain, the heavy and light hole bands are no longer degenerate at the gamma point ($k = 0$).

2.3.2. 1D Schrödinger equation

Once the new band edges and effective masses for each of the materials forming the quantum well structure are known, the quantum properties can be calculated by solving the 1 dimensional Schrödinger's equation. Solcore uses the method de-

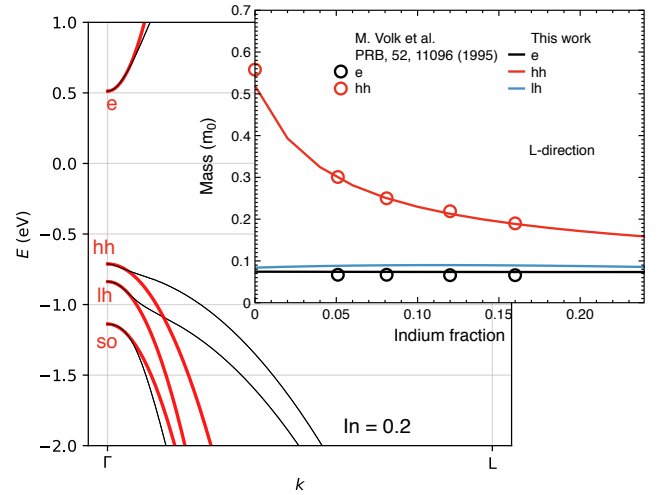


Figure 4: Band structure of $\text{In}_{0.2}\text{Ga}_{0.8}\text{As}$ calculated with the bulk kp solver. The inset shows the effective mass determined for a range of indium fractions and a comparison with the experimental data from Volk et al. [19]

scribed by Frensky [20] which allow to calculate the eigenvalues and eigenvectors of an arbitrary potential. A tridiagonal matrix is constructed by writing the variable effective mass Schrödinger's equation over a series of mesh points. The eigenvalues of the matrix correspond to the allowed energy levels of the system. Thus, the system of equations to solve over the meshpoints is given by:

$$\mathcal{H}\Psi_i = -s_i\Psi_{i-1} + d_i\Psi_i - s_{i+1}\Psi_{i+1} = E\Psi_i \quad (4)$$

where s_i and d_i depend on the mesh spacing Δ and the position dependent potential V_i and effective masses m_i as:

$$d_i = \frac{\hbar^2}{4\Delta^2 m_0} \left(\frac{1}{m_{i-1}} + \frac{2}{m_i} + \frac{1}{m_{i+1}} \right) + V_i \quad (5)$$

$$s_i = \frac{\hbar^2}{4\Delta^2 m_0} \left(\frac{1}{m_{i-1}} + \frac{1}{m_i} \right) \quad (6)$$

This system is solved using the tools available in the Scipy package for solving sparse linear systems of equations, in particular `sparse.linalg.eigs`.

Fig. 5 shows two examples of the band profile and wavefunctions calculated by Solcore. The first one (Fig. 5a and b) is a single InGaAs QW with GaAs interlayers and GaAsP barriers. The strain and the quantum confinement shift the light hole valence band (dashed line) with respect to the heavy hole valence band (continuous line). In the GaAsP barriers, under tensile strain, this shift is in the opposite direction than inside the QW, under compressive strain and the effects of confinement.

Fig. 5c and d shows the same information but for a multi-QW structure with thin barriers. For the electrons, there is strong coupling between the QWs, resulting in a range of energies for the ground state and the formation of a miniband. The heavy holes ground states are two deep, resulting in lower coupling between wells and a smaller broadening of the miniband.

2.4. Critical-Point Parabolic-Band Optical Constant Model

Understanding the optical response of both established and novel materials is crucial to effective solar cell design. To efficiently model the complex dielectric function of a material Solcore incorporates an optical constant calculator based on the well known Critical-Point Parabolic-Band (CPPB) formalism popularised by Sadao Adachi [21, 22, 23]. In this model contributions to $\epsilon_2(\omega)$ are considered at a number of critical points in the Brillouin Zone, at which the probability for optical transitions is large. The probability of such transitions are governed by the joint density of states (JDOS) function $\mathbf{J}_{cv}(\omega)$, which describes the number of available electronic states between the valence and conduction bands at given photon energy. The imaginary part of the complex dielectric function relates to the JDOS as;

$$\epsilon_2(\omega) = \frac{4\hbar^2 e^2}{\pi \mu_0^2 \omega^2} |\langle c|p|v \rangle|^2 \mathbf{J}_{cv}(\omega) \quad (7)$$

Where $|\langle c|p|v \rangle|$ is the momentum matrix element for transitions from the valence band (v) to the conduction band (c). Critical point transitions are considered at the following points of symmetry in the band structure; E_0 corresponds to the optical transition at the Γ point and $E_0 + \Delta_0$ the transition from the spin-orbit split off band to the conduction band. E_1 and $E_1 + \Delta_1$ denotes the transitions from the valence heavy-hole (HH) band and the valence light-hole (LH) band to the conduction band respectively at the L point. The E'_0 triplet and E_2 transitions occur at higher energies, between the HH band and the split conduction bands at the Γ point as well as across the wide gap X valley. The model also includes contributions from the lowest energy indirect band-gap transition and also exciton absorption at the E_0 critical point. The contributions listed above are summed to compute the overall value of $\epsilon_2(\omega)$. The real and imaginary components of the overall complex dielectric function $\epsilon(\omega) = \epsilon_1(\omega) + i\epsilon_2(\omega)$ are thus related via the Kramers-Krönig relations;

$$\epsilon_1(\omega) = 1 + \frac{2}{\pi} \int_0^\infty \frac{\omega' \epsilon_2(\omega')}{(\omega')^2 - \omega^2} d\omega' \quad (8)$$

$$\epsilon_2(\omega) = -\frac{2}{\pi} \int_0^\infty \frac{\epsilon_1(\omega')}{(\omega')^2 - \omega^2} d\omega' \quad (9)$$

The CPPB model included with Solcore also incorporates a modification to the critical point broadening present in Adachi's description, which is shown to produce a poor fit to experimental data in the vicinity of the E_0 and E_1 critical points [24]. To give a more accurate description of the broadening of the optical dielectric function, Charles Kim proposed that a frequency dependent damping parameter be used to replace the damping constant given by Adachi at each critical point [25, 26];

$$\Gamma'(\omega) = \Gamma \exp \left[-\alpha \left(\frac{\hbar\omega - E_0}{\Gamma} \right)^2 \right] \quad (10)$$

Where Γ is the damping constant used by Adachi and α describes the shape of the lineshape broadening with $\alpha = 0$ producing purely Lorentzian character and $\alpha = 0.3$ producing a good approximation to Gaussian broadening.

The Solcore module `absorption_calculator` contains the CPPB model within the `Custom_CPPB` class. The class offers a flexible way to build up the optical constant model by adding individual critical point contributions through the *Oscillator* structure type within Solcore. In addition to the oscillator functions described by Adachi the `Custom_CPPB` class also provides additional oscillator models and the Sellmeier equation for describing the real part of the dielectric function for non-absorbing materials [27]. Below is some example code that calculates the optical dielectric function of GaAs;

```
from solcore.absorption_calculator.Custom_CPPB import Custom_CPPB
import numpy as np
```

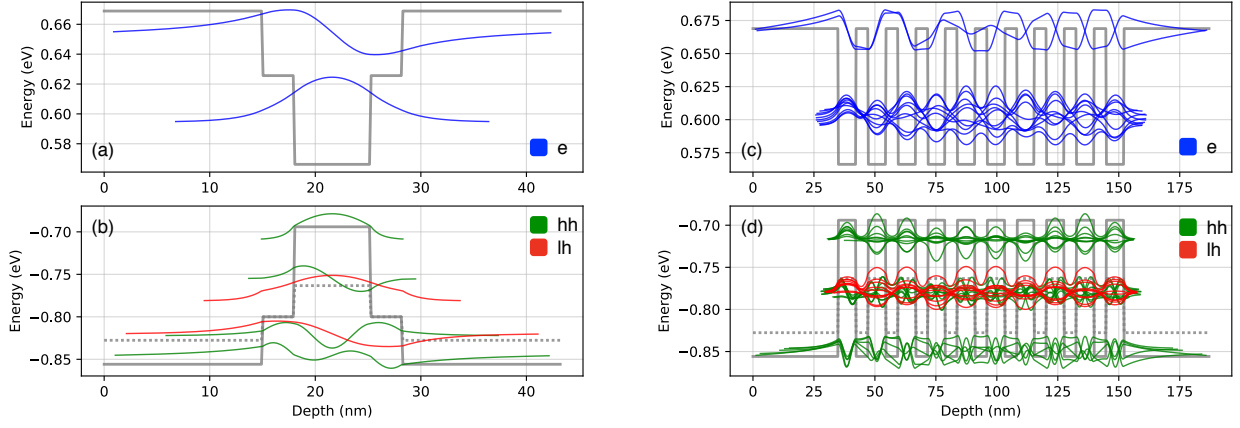


Figure 5: Band profile of (a), (b) a single InGaAs QW with GaAs interlayers and GaAsP barriers and (c), (d) a multi-QW structure with 10 coupled QWs.

```
# Generate a list of energies over which to calculate the model dielectric function.
E = np.linspace(0.2, 5, 1000)

# Class object is created, CPPB_Model
CPPB_Model = Custom_CPPB()

# The MatParams method loads in the desired material parameters as a dictionary variable.
MatParams = CPPB_Model.Material_Params("GaAs")

# The oscillator type and material parameters are both passed to individual oscillators in the
# 'Oscillator' structure.
Adachi_GaAs = Structure([
    Oscillator(oscillator_type="E0andE0_d0", material_parameters=MatParams),
    Oscillator(oscillator_type="E1andE1_d1", material_parameters=MatParams),
    Oscillator(oscillator_type="E_ID", material_parameters=MatParams),
    Oscillator(oscillator_type="E2", material_parameters=MatParams)
])

Output = CPPB_Model.eps_calc(Adachi_GaAs, E)
```

Listing 2: Modelling of the n and k based on the CPPB model.

Figure 6 shows the real and imaginary components of the complex dielectric function of GaAs as calculated by the Custom_CPPB class. The model shows excellent agreement with the experimental data taken from Palik [28] and using a set of parameters for GaAs similar to those specified in [22]. For a recent demonstration of Solcore's CPPB model, please refer to this discussion on *'The effects of short-range alloy disorder on the voltage performance of potential GaAsBi based solar cells'* in [29].

2.5. QW absorption calculator

For modelling the optical properties of QWs we use the method described by S. Chuang [Chuang Book 2009]. The absorption coefficient at thermal equilibrium in a QW is given by:

$$\alpha_0(E) = C_0(E) \sum_{n,m} |I_{nm}^{en}|^2 |\hat{e} \cdot \vec{p}|^2 \rho_r^{2D} [H(E - E^{en} + E_{hm}) + F_{nm}(E)] \quad (11)$$

where $|I_{nm}^{en}|^2$ is the overlap integral between the holes in level m and the electrons in level n ; H is a step function, $H(x) = 1$ for

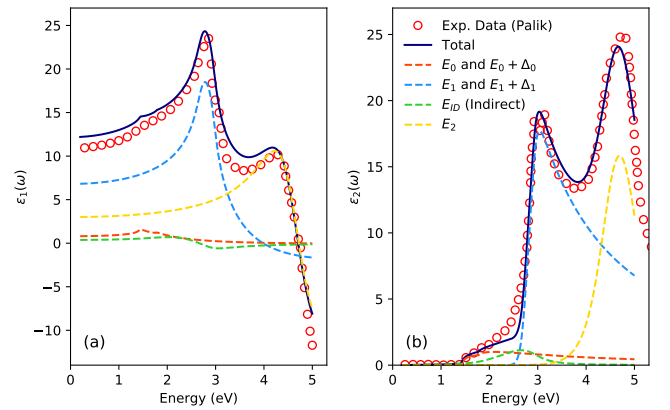


Figure 6: Output of the CPPB model provided by Solcore fit to existing experimental data from Palik [28]

| | TE | TM |
|----------|------------|----------|
| $c - hh$ | $3/2M_b^2$ | 0 |
| $c - lh$ | $1/2M_b^2$ | $2M_b^2$ |

Table 1: Momentum matrix elements for transitions in QWs. $M_b^2 = m_0 E_p / 6$ is the bulk matrix element.

$x > 0$, 0 and 0 for $x < 0$; ρ_r^{2D} is the 2D joint density of states; C_0 a proportionality constant dependent on the energy; and F the excitonic contribution, that will be discussed later.

$$C_0(E) = \frac{\pi q^2 \hbar}{n_r c \epsilon_0 m_0^2 E} \quad (12)$$

$$\rho_r^{2D} = \frac{m_r^*}{\pi \hbar L} \quad (13)$$

Here, n_r is the refractive index of the material, $m_r = m_e m_h / (m_e + m_h)$ the reduced effective mass and L an effective period of the quantum wells. $|\hat{e} \cdot \vec{p}|^2$ is the momentum matrix element, and it depends on the polarization of the light and on the Kane's energy E_p , specific of each material and determined experimentally. For the band edge absorption, where $k = 0$, the matrix elements for the absorption of TE and TM polarized light for the transitions involving the conduction band and the heavy and light holes bands are given in Table 1. As it can be deduced from this table, transitions involving heavy holes can not absorb TM polarised light.

In addition to the band-to-band transitions, QWs usually have a strong excitonic absorption, included in Eq. 12 in the term F_{nm} . This term is a Lorentzian (or Gaussian) defined by an energy $E_{nm,j}$ and oscillator strength $f_{ex,j}$. It is zero except for $m = n \equiv j$ where it is given by Klipstein et al. [30]:

$$F_{nm} = f_{ex,j} \mathcal{L}(E - E_{nm,j}, \sigma) \quad (14)$$

$$E_{nm,j} = E^{en} - E_{hm} - \frac{R}{(j - \nu)^2} \quad (15)$$

$$f_{ex,j} = \frac{2R}{(j - \nu)^3} \quad (16)$$

$$R = \frac{m_r q^4}{2(4\pi\epsilon_r\epsilon_0)^2 \hbar^2} \quad (17)$$

Here, ν is a constant with a value between 0 and 0.5 and σ is the width of the Lorentzian, both often adjusted to fit some experimental data. In Solcore, they have default values of $\nu = 0.15$ and $\sigma = 6$ meV. R is the exciton Rydberg energy [31].

Fig. 7 shows the absorption coefficient of a range of InGaAs/GaAsP QWs with a GaAs interlayer and different In content. Higher indium content increases the depth of the well, allowing the absorption of less energetic light and more transitions.

3. Light sources

Transforming sunlight into electricity is the final goal of any solar cell and it is therefore necessary to have a convenient way

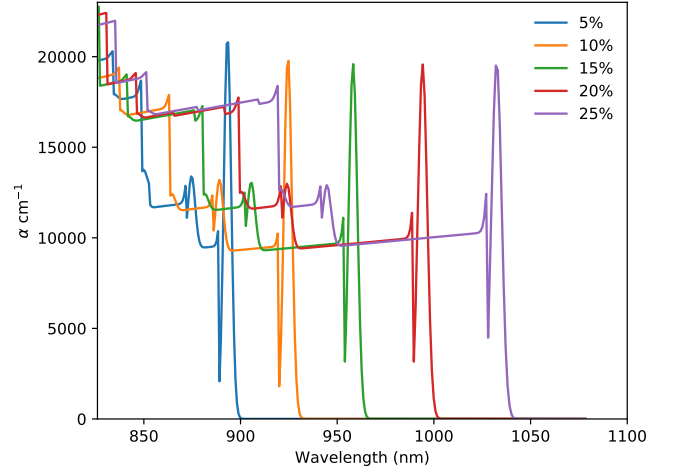


Figure 7: QW absorption coefficient as a function of the indium content.

of creating, manipulating and modifying the properties of the spectrum of the light. Ideally, solar cells will be designed and evaluated under a standard solar spectrum - eg. the air mass 1.5 direct solar spectrum, AM1.5D - but practical light sources are not standard. More often than not, we will be interested in modelling the performance of a solar cell under the experimental spectrum of a solar simulator or lamp in a laboratory, simulated data calculated from atmospheric conditions (temperature, humidity, aerosol content, etc.) or even under real irradiance data measured at different locations worldwide. This can then be compared with the experimental performance or tailored to work best under certain conditions.

The Solcore module `light_source` is designed to deal easily with different light sources. It has direct support for:

- Gaussian emission, typical of lasers and light emitting diodes.
- Black body radiation, characteristic of halogen lamps defined by a temperature, but also used very often to simulate the spectrum of the Sun, very close to a black body source at 5800 K.
- Standard solar spectra: the extraterrestrial spectrum AM0 and the two terrestrial ones, AM1.5D and AM1.5G as defined by the ASTM G173 - 03(2008) standard.
- Irradiance models, using location, time and atmospheric parameters to calculate a synthetic solar spectrum. Solcore includes two models: SPECTRAL2, fully implemented in python, and an interface to SMARTS binaries (need to be installed separately), which greatly simplifies its use in batch mode.
- User-defined irradiances, provided externally from a database or any other source, allowing for a maximum flexibility.

The syntax in all cases is simple and intuitive considering the type of source that needs to be created. In the case of the irradiance models, which often have a large number of inputs, Solcore defines a set of default values, so only those that are dif-

ferent need to be provided. The code in Listing 3 illustrates the creation of several light sources using the minimum required input in each case. A plot of those light sources is shown in Figure 8.

```
import numpy as np
from solcore.light_source import LightSource

#The wavelength range of the spectra
wl = np.linspace(300,3000,200)

gauss = LightSource(source_type='laser',x=wl,center=800,linewidth=50,power=200)
bb = LightSource(source_type='black body',x=wl,T=5800,entendue='Sun')
am15g = LightSource(source_type='standard',x=wl,version='AM1.5g')
smarts = LightSource(source_type='SMARTS',x=wl)
spectral = LightSource(source_type='SPECTRAL2',x=wl)
```

Listing 3: Example of the use of the LightSource class.

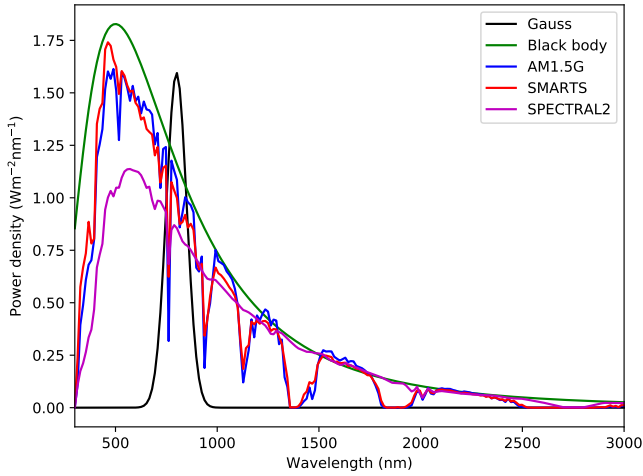


Figure 8: Plot of the spectra of different light sources

Once created, specific parameters of the light sources can be easily modified without the need for creating the source from scratch. That is particularly useful for the irradiance models where we might be interested in getting the spectrum as a function of certain parameter (eg. the hour of the day, or the humidity) without changing the others. For example, `smarts.spectrum(HOUR=11)` and `smarts.spectrum(HOUR=17)` will provide the spectrum of the SMART light source defined above calculated at 11h and at 17h, respectively; all additional parameters have the default values. This method has been used to model experimental solar irradiances measured by different spectroradiometers based on the local atmospheric conditions [32].

A final, very convenient feature of the LightSource class is the possibility of requesting the spectrum in a range of different units. De default is power density per nanometer, but other very common units are power density per eV or photon flux per nanometer, among others. While these unit conversions are

straight forward, it is often an initial source of errors due to missing constants or incompatible magnitudes.

The `light_source` module has been described in the context of the solar spectrum, but it can be applied broadly where there is spectral data involved, such as the fitting of photoluminescence, electroluminescence or Raman spectra.

4. Optical solvers

The purpose of the optical solvers is to obtain the fraction of incoming light reflected, absorbed and transmitted in a solar cell as a function of the wavelength of the light and the position inside the structure. Solcore includes three models to tackle this problem: Beer-Lambert law (BL), transfer matrix method (TMM) and rigorous wave coupled analysis (RWCA). At the moment, Solcore does not have explicit support for light trapping effects using general textured surfaces, as it is the usual situation in silicon solar cells. However, this can be implemented to a large extent using the RWCA method, although not very efficiently. It also accepts as inputs the reflection, transmission and absorption as a function of the position in the structure, allowing to use external tools to solve complex photonic structures.

All the optical solvers apply to the solar cell structure as a whole, providing as output the fraction of light reflected $R(\lambda)$, transmitted $T(\lambda)$ and absorbed per unit length at a depth z from the front surface $A(\lambda, z)$.

4.1. Beer-Lambert law (BL)

This is the simplest model to calculate the absorption in a multilayer structure. It ignores all reflection in the interfaces - the front surface reflection can be provided externally and it is zero otherwise at all wavelengths - and the absorption per unit length as a function of the wavelength λ and the position z in layer n is given by:

$$A_n(\lambda, z) = \alpha_n(\lambda) \exp \left(- \sum_{i=1}^{n-1} \alpha_i(\lambda) w_i - \alpha_n(\lambda)(z - z_n) \right) \quad (18)$$

where α_n is the absorption coefficient of layer n , w_n its thickness and z_n the position of the beginning of the layer. Due to its simplicity, the BL law is used widely in photovoltaics but in reality it is only applicable when the contrast in the refractive index between layers can be ignored and when there is strong absorption, reducing the effects of light reflection at the interfaces. .

4.2. Transfer matrix method (TMM)

In order to evaluate the realistic optical behaviour of a potential solar cell design it is important to consider the interaction of incident electromagnetic (EM) radiation with a succession of both absorbing and non-absorbing planar layers. The combined optical response of such a layered structure is crucial when considering the minimisation of extrinsic front surface reflection losses [33], the emissivity in the mid-IR of low emissivity coatings for hybrid PV-thermal applications [34] and also when studying the optical constants and layer thicknesses of material using the experimental technique of spectroscopic ellipsometry. Therefore, Solcore evaluates the interaction of incident EM radiation through a layered structure using the Transfer Matrix Method (TMM). The incident light radiation takes the form of homogeneous, electromagnetic plane-polarised waves and is represented by components describing the electric, \mathbf{E} and magnetic field strengths, \mathbf{H} ;

$$\mathbf{E} = \mathcal{E} \exp \left[i\omega t - \left(\frac{2\pi N}{\lambda} \right) z + \varphi \right] \quad (19)$$

$$\mathbf{H} = \mathcal{H} \exp \left[i\omega t - \left(\frac{2\pi N}{\lambda} \right) z + \varphi' \right] \quad (20)$$

Where \mathcal{E} and \mathcal{H} denote the electric and magnetic field amplitudes respectively, N the complex refractive index, z the distance in the direction of propagation, ω the angular frequency and λ the wavelength of radiation. φ and φ' both represent an

arbitrary phase angle for both the electric and magnetic travelling wave components and are not independent of each other. The characteristic transfer matrix for evaluating the interaction between planar electric and magnetic waves at the interface of n thin films on a semi-infinite substrate is derived in detail elsewhere [35] and given by the equation;

$$\begin{bmatrix} \mathbf{E} \\ \mathbf{H} \end{bmatrix} = \left\{ \prod_{q=1}^n \begin{bmatrix} \cos(\delta_q) & [i \sin(\delta_q)]/\eta_q \\ i\eta_q \sin(\delta_q) & \cos(\delta_q) \end{bmatrix} \right\} \begin{bmatrix} 1 \\ \eta_m \end{bmatrix} \quad (21)$$

Where δ_q is defined as the phase factor of the q_{th} planar layer, η_q the optical admittance of the q_{th} layer and η_m the optical admittance of the substrate. The layer closest to the incident medium is evaluated first before working through the n layer structure in order. The term δ_q describes the phase shift required to translate the z coordinate of the E and H interactions by the thickness of each layer, q . The spectrally varying fresnel coefficients describing reflection, transmission and absorption of the multi-layer structure can be calculated from the solutions to equation 21 at discrete wavelengths;

$$R = \left(\frac{\eta_0 \mathbf{E} - \mathbf{H}}{\eta_0 \mathbf{E} + \mathbf{H}} \right) \left(\frac{\eta_0 \mathbf{E} - \mathbf{H}}{\eta_0 \mathbf{E} + \mathbf{H}} \right)^* \quad (22)$$

$$T = \frac{4\eta_0 \text{Re}(\eta_m)}{(\eta_0 \mathbf{E} + \mathbf{H})(\eta_0 \mathbf{E} + \mathbf{H})^*} \quad (23)$$

$$A = \frac{4\eta_0 \text{Re}(\mathbf{E}\mathbf{H}^* - \eta_m)}{(\eta_0 \mathbf{E} + \mathbf{H})(\eta_0 \mathbf{E} + \mathbf{H})^*} \quad (24)$$

The implementation of the TMM in Solcore uses the freely available `tmm` module developed by Byrne [36]. The multi-layer optical stack is built up using Solcore's *Structure* object. Some example code evaluating the TMM for a triple layer anti-reflection coating (ARC) on top of conventional multi-junction solar cell materials AlInP and GaInP is included below in Listing 4.

```
# The optical stack is built defining layer thickness, wavelength range and material
# n and k data.
OptiStack = Structure([
    [117, 1240/E_eV, mgf_nk[1], mgf_nk[2]],
    [80, 1240/E_eV, sic_nk[1], sic_nk[2]],
    [61, 1240/E_eV, zns_nk[1], zns_nk[2]],
    [25, 1240/E_eV, alinp_nk[1], alinp_nk[2]],
    [350000, 1240/E_eV, gainp_nk[1], gainp_nk[2]]
])

# The Reflection, Transmission and Absorption is evaluated for a range of incident
# angles (in degrees).
angles = np.linspace(0, 80, 10)
RAT_angles = []

for theta in angles:

    rat_data = []
    # Calculate RAT data...
    rat_data = calculate_rat(OptiStack, angle=theta, wavelength=1240 / E_eV)

    RAT_angles.append((theta, rat_data["R"], rat_data["A"], rat_data["T"]))
```

Listing 4: Calculation of the reflection, absorption and transmission of a structure.

Figure 9a depicts calculated reflection and transmission from the solutions to the characteristic TMM equation over a range of incident angles for an optimised triple layer ARC design reported in [33]. The solid lines indicate the optical reflection at the front surface whilst the dashed lines correspond to the transmitted light into the substrate, in this case taken to be the optically thick top sub-cell material of GaInP.

In addition to using the TMM for calculating the reflection, transmission and absorption in a multi-layer optical stack it can also be applied to the popular spectroscopic technique of ellipsometry. This measures a change in the polarisation of incident light reflected at the surface of a sample under test. A more detailed description regarding the ellipsometry technique and its uses is described elsewhere. The measured values are expressed as Psi (Ψ) and Delta (Δ) and relate to the s and p components of the fresnel coefficient R by;

$$\rho = \frac{R_p}{R_s} = \tan(\Psi)e^{i\Delta} \quad (25)$$

As the ratio between p and s components of R is a com-

plex quantity phase change information is contained within the imaginary part of equation 25 (Δ). The change in phase of the reflected electric and magnetic plane waves can be evaluated from the solution of equation 21 and is given by;

$$\varphi = \arctan\left(\frac{\text{Im}[\eta_m(\mathbf{E}\mathbf{H}^* - \mathbf{H}\mathbf{E}^*)]}{(\eta_m^2\mathbf{E}\mathbf{E}^* - \mathbf{H}\mathbf{H}^*)}\right) \quad (26)$$

The complex dielectric function of the sample can be calculated from the experimental ellipsometry result with the solutions to equation 25:

$$\langle\epsilon\rangle = \epsilon_1 + i\epsilon_2 = \sin(\theta) \left[1 + \tan^2(\theta) \left(\frac{1 - \rho}{1 + \rho} \right)^2 \right] \quad (27)$$

Some example code, calculating the complex dielectric function from the ellipsometric response of a sample of Ge substrate is summarised below. The output of the model is shown in Figure 9b as the dashed line and is compared with experimentally obtained data at an incident angle of 79°. Good agreement with the experimental data is observed when a thin, roughly 4.5 nm, layer of Germanium Oxide is included in the layer model.

```
from solcore.absorption_calculator import calculate_ellipsometry
from solcore.structure import Structure

# Input array of energies (in eV).
E_eV = np.linspace(0.7, 4.2, 1000)

Define the optical stack structure, a piece of Ge substrate with a thin Ge oxide layer.
# Layer 1 :: GeO2 native oxide layer
# Substrate :: Bulk Ge
OptiStack = Structure([
    [4.5, 1240/E_eV, GeO2_nk["n"], GeO2_nk["k"]],
    [350000, 1240/E_eV, Ge_nk["n"], Ge_nk["k"]]
])

# Calculate ellipsometry variables, Psi and Delta
Exp_Angles = [75, 77, 79]
Out = calculate_ellipsometry(OptiStack, 1240/E_eV, angle=Exp_Angles)

# Modelled data...
Mod_rho = rho(np.radians(Out["psi"][:,i]), np.radians(Out["Delta"][:,i]))
Mod_eps = eps(Mod_rho, np.radians(Exp_Angles[i]))
```

Listing 5: Example of the calculation of the ellipsometric Ψ and Δ .

4.3. Rigorous wave couple analysis (RWCA)

Finally, Solcore includes an interface to the S^4 solver, developed at the Stanford University, in order to model solar cells with nanophotonic designs [37]. S^4 uses the RWCA algorithm to solve the linear Maxwell's equations in structures containing 2D and 3D periodicity, in contrast to the TMM, which only solves 1D periodic structures. Such structures can be found in advanced solar cell designs aiming, for example, to reduce the solar cell thickness by scattering the incoming light sideways using an array of periodic, metallic nanoparticles in the front surface.

5. Single junction solar cells

Solcore includes four solvers to calculate the electrical properties of a single junction device. In order of increasing accuracy, they are: detailed balance, 2-diode equation, depletion approximation and Poisson-drift-diffusion.

5.1. Detailed balance (DB)

This solver calculates the electrical properties of the junction by balancing the elementary processes taking place in the solar cell, carrier generation and radiative recombination, using the formalism described by Araújo and Martí [38]. The method

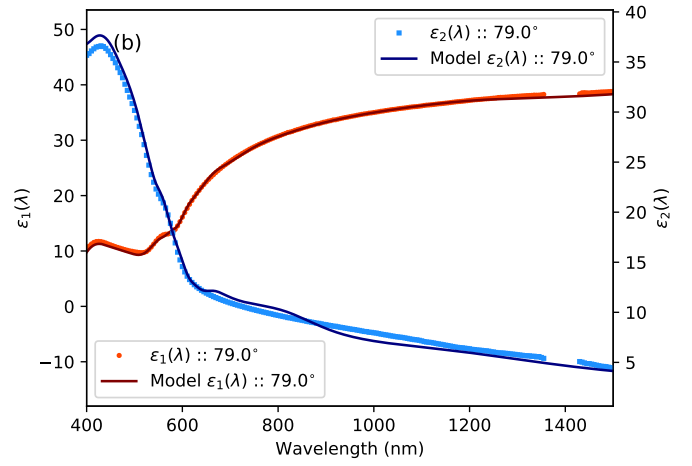
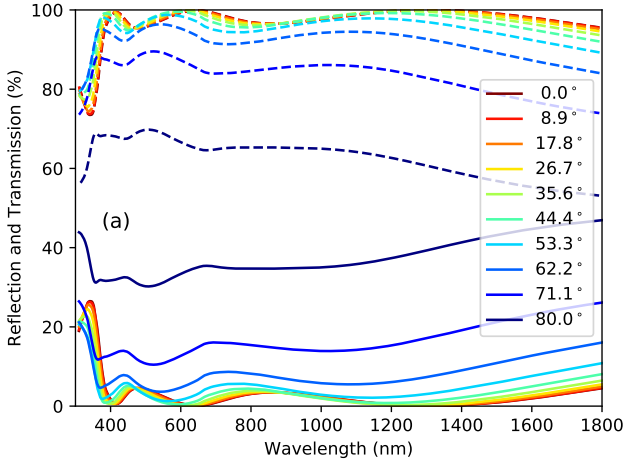


Figure 9: Example solutions from the TMM module in Solcore calculating Reflection, Transmission and complex dielectric function. (a) Spectral reflection (solid lines) and transmission (dashed lines) over a range of angles for the optimised triple layer ARC reported in [33]. (b) The calculated real and imaginary components of the complex dielectric function obtained from spectroscopic ellipsometry of a Ge substrate at 79°. The simulated result is depicted by the dashed lines.

is widely used by the photovoltaic community to calculate the limiting conversion efficiencies of the different solar cell architectures or materials. The simplest DB formulation only needs an absorption edge energy and an absorptivity value above that edge. Out of this, the carrier generation and radiative recombination are calculated for different internal chemical potentials, equal to the external electrical bias, in the ideal case. Solcore includes this basic model, but also allows the user to provide a more complex absorption profile.

The radiative recombination or thermal generation current J_{rad} from the solar cell is calculated following the formalism described by Nelson et al. [14], considering all the possible paths of the light absorbed by the cell and the reciprocity relation between emission and absorption. The total radiative current, using the generalized Planck's equation, is given by:

$$J_{rad}(V, T) = q \frac{2n^2}{h^3 c^2} \int_0^\infty \frac{E^2}{e^{\frac{E-qV}{k_b T}} - 1} \left[\int_S A(E, \theta, \vec{s}) d\Omega d\vec{s} \right] dE$$

$$= q \frac{2n^2}{h^3 c^2} \int_0^\infty \frac{E^2}{e^{\frac{E-qV}{k_b T}} - 1} [A_{front}(E) + A_{back}(E)] dE \quad (28)$$

where $A(E, \theta, \vec{s})$ is the probability that a photon of energy E will be emitted (absorbed) from the point \vec{s} on the surface at an internal angle θ , and $A_{front}(E)$ and $A_{back}(E)$ the combined probability of the photon to be emitted (absorbed) by the front and the back of the cell, respectively.

The different paths of the absorbed light are depicted in Fig. 10. Path A represents light that reaches the front surface within the escape cone ($\theta < \theta_c$) and that crosses the structure. Path B is the light that reaches the back surface outside the escape cone of the front surface ($\theta > \theta_c$), being totally internally reflected and crossing the structure twice. Light reaching the back surface within the escape cone ($\theta < \theta_c$) can either escape through the front (path C) or be reflected (path D). With these consider-

ations, the contribution to the surface integral of the four terms will be [Nelson 1997]:

$$A - 2\pi S_{front} \int_{\cos \theta_c}^1 [1 - r(E, \theta)] (1 - e^{-\alpha w / \cos \theta}) \cos \theta d(\cos \theta)$$

$$B - 2\pi S_{back} \int_0^{\cos \theta_c} (1 - e^{-2\alpha w / \cos \theta}) \cos \theta d(\cos \theta)$$

$$C - 2\pi S_{back} \int_{\cos \theta_c}^1 [1 - r(E, \theta)] (1 - e^{-\alpha w / \cos \theta}) \cos \theta d(\cos \theta)$$

$$D - 2\pi S_{back} \int_{\cos \theta_c}^1 r(E, \theta) (1 - e^{-2\alpha w / \cos \theta}) \cos \theta d(\cos \theta) \quad (29)$$

These equations can be written in a more compact form by noting that $r = 1$ for $\theta > \theta_c$. In this situation, B, C and D can be combined and the integral extended from 0 to 1, resulting simply in:

$$A_{back}(E) = 2\pi \int_0^1 [1 + r(E, \theta) e^{-\alpha w / \cos \theta}] \times (1 - e^{-\alpha w / \cos \theta}) \cos \theta d(\cos \theta) \quad (30)$$

The factor S_{back} representing the area of the back of the cell has been omitted here as we are interested in the current density, and therefore independent of the area. Likewise, $A_{front}(E)$ will be given simply by the component A in Eq. 29:

$$A_{front}(E) = 2\pi \int_{\cos \theta_c}^1 [1 - r(E, \theta)] (1 - e^{-\alpha w / \cos \theta}) \cos \theta d(\cos \theta) \quad (31)$$

$J_{rad}(V, T_{cell})$ will represent the radiative recombination of the cell at a bias V and temperature T_{cell} while $J_{rad}(0, T_a)$ will be the carrier generation due to thermal radiation from the ambient at a temperature T_a . Typically, $T_{cell} = T_a$.

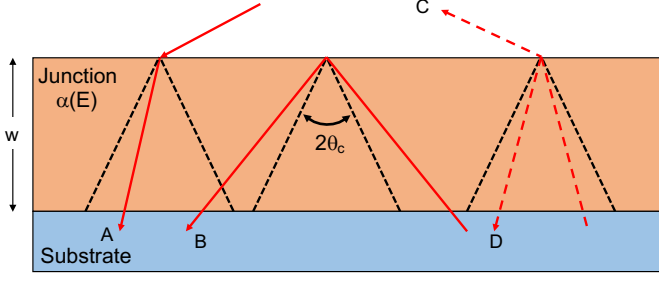


Figure 10: All the paths that radiation can follow within the cell, used to calculate the absorptivity=emissivity as a function of the angle.

Carrier generation in the solar cell due to the absorption of the solar irradiance $H(E)$ can be written simply as:

$$J_{sc} = q \int_0^\infty [1 - R(E)] A_n(E) H(E) dE \quad (32)$$

with A_n the normal incidence absorptivity of the cell that, $A(E) = 1 - \exp(-\alpha(E)w)$ with w the thickness of the junction, α the absorption coefficient and $R = r(E, 0)$ the normal incidence reflection.

Combining all these equations, the total current as a function of the bias calculated with the DB model will be given by:

$$J = J_{sc} + J_{rad}(0, T_a) - J_{rad}(V, T_{cell}) \quad (33)$$

If $T_a = T_{cell}$ and $E \gg k_b T$, Eq. 33 simplifies, resulting in:

$$J = J_{sc} - J_{01} \left(e^{\frac{qV}{k_b T_{cell}}} - 1 \right) \quad (34)$$

with J_{01} the reverse saturation current, given by:

$$J_{01} = q \frac{2n^2}{h^3 c^2} \int_0^\infty E^2 e^{-\frac{E}{k_b T_{cell}}} [A_{front}(E) + A_{back}(E)] dE \quad (35)$$

While in these equations the term $\exp(\alpha w)$ is used, it should be noted that none of the two parameters are needed as the product is calculated internally by Solcore from the normal incidence absorptivity $A_n(E)$, which is the value given as input:

$$e^{-\alpha w} = 1 - A_n(E) \quad (36)$$

5.2. 2-diode model (2D)

This is the simplest method of simulating the behaviour of a solar cell, using electrical components to model the different transport and recombination mechanisms of the device. The usual representation models the photocurrent as a current source (J_{sc}), radiative and non-radiative recombination modelled as diodes (with parameters J_{01} and n_1 , J_{02} and n_2 , respectively) and shunt and series resistances to account for the other transport losses (R_s and R_{sh}). While R_s needs to be defined when creating the junction, it is included in the calculation at solar cell level, and not at junction level (see Section 6).

$$J = J_{sc} - J_{01} \left(e^{\frac{qV}{n_1 k_b T}} - 1 \right) - J_{02} \left(e^{\frac{qV}{n_2 k_b T}} - 1 \right) - \frac{V}{R_{sh}} \quad (37)$$

In Solcore, the parameters of Equation 37 might have different origins. They can be directly provided as input, obtained from the fitting to experimental data, for example. But they can also be calculated internally, using the DB solver to obtain J_{01} and J_{sc} , and then use a radiative efficiency coefficient to obtain J_{02} . The radiative efficiency η is defined as the fraction of radiative current J_{rad} at a given reference total current J_{ref} :

$$\eta = \frac{J_{rad}}{J_{ref}} = \frac{J_{01}}{J_{ref}} \left(e^{\frac{qV_{ref}}{n_1 k_b T}} - 1 \right) \quad (38)$$

The reference voltage V_{ref} can be written as a function of η and J_{ref} as:

$$V_{ref} = \frac{n_1 k_b T}{q} \log \left(\frac{\eta J_{ref}}{J_{01}} + 1 \right) \quad (39)$$

On the other hand, the radiative coefficient can also be written as:

$$\eta = \frac{J_{ref} - J_{nrad} - V_{ref}/R_{sh}}{J_{ref}} \quad (40)$$

Combining Eq. 39 and 40 and using the expression for the diode with ideality factor n_2 , J_{02} can be written as:

$$J_{02} = \frac{(1 - \eta) J_{ref} - V_{ref}/R_{sh}}{e^{\frac{qV_{ref}}{n_2 k_b T}} - 1} \quad (41)$$

In the common situation of very large shunt resistance and $V_{ref} \gg k_b T/q$, this equation further simplifies to:

$$J_{02} = (1 - \eta) J_{ref} \left(\frac{J_{01}}{J_{ref} \eta} \right)^{n_1/n_2} \quad (42)$$

This process can, of course, be reversed and use the knowledge of J_{01} and J_{02} at a given reference current to calculate the radiative efficiency of a solar cell, useful to compare different materials, technologies or processing methods. This was done by Chan et al. using $J_{ref} = 30 \text{ mA/cm}^2$, obtaining η values of 20% for InGaP, 22% for GaAs, and 27% for InGaAs devices [39]. Despite the simplicity of the 2-diode model, it is very useful to guide the design of new solar cells and explore the performance of new materials, such as doped bismuth alloys [40], or to assess the performance of large arrays of solar cells, as it will be shown in Section 7 [41].

5.3. Poisson-drift-diffusion (PDD)

This method solves the Poisson equation for the electrostatic potential coupled with the transport equations for electrons and holes and suitable boundary conditions in the steady state. It is the standard method for calculating the electrical properties of most semiconductor devices, including solar cells, transistors or light emitting diodes. It is also the only method included in most software packages for simulating semiconductor devices, such as PC-1D [42], Nextnano or AFORS-HET. It is generally

considered a hard problem to solve due to the broad range of variation that the variables have across the structure, especially in the presence of discontinuities in the band structure.

Figure 11a shows the flow chart of Solcore's PDD solver. Any simulation starts by calculating the band structure under equilibrium conditions (no illumination or bias). If the simulation includes illumination, the photogeneration as a function of the position in the structure is calculated externally to the PDD solver using any of the models described in Section 4. To aid convergence, the solution at short circuit conditions is calculated by increasing the light intensity from zero to the nominal value in small steps. Similarly, the solution at any bias is obtained by solving the problem first at zero bias and then increasing it in small steps, using the previous solution as the initial condition for the next one. Re-meshing is performed in several occasions during the simulation of the current-voltage characteristics (see section 5.3.3).

To calculate the internal quantum efficiency (IQE), a small differential increase is included in the photogeneration profile as a function of wavelength. The IQE is then calculated as the ratio between the resulting increase in the photocurrent and the increase in the photogeneration at that wavelength. This procedure is comparable to the actual experimental measurement of the quantum efficiency.

5.3.1. Solver assumptions and formulation

The Poisson's and drift-diffusion equations relate the electrostatic potential created by the free and fixed charges with the carrier densities and their variation across the structure due to generation, recombination and externally applied bias. The reader is referred to any semiconductors textbook for a detailed description of their derivation (see for example [43] or [44]). The solver uses the Boltzmann approximation with the following assumptions:

- There is no carrier-carrier scattering.
- All carrier populations are in thermal equilibrium.
- The mobility of carriers is independent of the electric field.
- Temperature is uniform.
- There are no magnetic fields.
- The structure of the energy levels available to the carriers is independent of the carrier density.

The Poisson's equation relates the electrostatic potential ϕ and the electrical charges in the structure. In one dimension, it can be written as:

$$\frac{d}{dx} \left(\epsilon \frac{d\phi}{dx} \right) + q(p - n + N_D - N_A) = 0 \quad (43)$$

where N_A , N_D , n and p are the density of ionized acceptors, donors, the density of free electrons and holes, respectively, and ϵ the dielectric constant. The current density equations account for the movement of carriers due to the electric field (drift

component) and to the carrier concentration gradient (diffusion component):

$$J_n = q\mu_n \left(nF + \frac{k_b T}{q} \frac{dn}{dx} \right) \quad (44)$$

$$J_p = q\mu_p \left(pF + \frac{k_b T}{q} \frac{dp}{dx} \right) \quad (45)$$

with μ is the carrier mobility and $F = -d\phi/dx$ the electric field. Finally, the continuity equations ensure particle conservation, balancing the carriers that enter and leave any point of the structure. Under steady state, this means that the variation of the current must be equal to the generation G and recombination R processes, which are equal for electrons and holes since they are created and annihilated in pairs:

$$\frac{dJ_n}{dx} + qG - qR = 0 \quad (46)$$

$$-\frac{dJ_p}{dx} + qG - qR = 0 \quad (47)$$

Combining Eq. 44, 45, 46 and 47 results in:

$$q\mu_n \left(\frac{k_b T}{q} \frac{d^2 n}{dx^2} + F \frac{dn}{dx} + n \frac{dF}{dx} \right) + qG - qR = 0 \quad (48)$$

$$q\mu_p \left(\frac{k_b T}{q} \frac{d^2 p}{dx^2} - F \frac{dp}{dx} - p \frac{dF}{dx} \right) + qG - qR = 0 \quad (49)$$

The Poisson's equation (Eq. 43) and the continuity equations (Eq. 48 and Eq. 49), together with the definitions for n , p and R , represent the complete system that needs to be solved in order to obtain the performance of the solar cell. The PDD solver included in Solcore uses the same discretization scheme used by PC-1D [Basore 1988 and PC-1D manual] taking as independent variables the electrostatic potential ϕ and the quasi-Fermi potentials for electrons and holes, ϕ_n and ϕ_p , respectively. These three variables are continuous across the whole structure and have comparable magnitudes, in the voltage range. Details of the discretization process are included in [45, 42], but they are based on minimising the total electrostatic energy in the case of the Poisson's equation, and in the Scharfetter-Gummel discretization scheme for the drift-diffusion equations [46].

The bulk recombination models included in Solcore are Shockley-Read-Hall recombination, radiative recombination and Auger recombination, as well as a surface recombination velocity model for the recombination at the contacts. These three recombination models are given by the following equations, respectively:

$$R_{SRH} = \frac{pn - n_i^2}{\tau_n(p + n_i) + \tau_p(n + n_i)} \quad (50)$$

$$R_{RAD} = B(pn - n_i^2) \quad (51)$$

$$R_{AUG} = (C_n n + C_p p)(pn - n_i^2) \quad (52)$$

with τ_n and τ_p the non radiative lifetimes of electrons and holes, B the radiative recombination coefficient and C_n and C_p the Auger recombination coefficient for electrons and holes.

At the moment, Solcore's PDD solver can not include interface charges or bandgap narrowing due to heavy doping and only implements ohmic contacts. Additionally, it only includes local carrier recombination processes and therefore can not deal with tunnel transport, which relates remote nodes.

This is the only part of Solcore implemented in Fortran using quadruple precision variables in order to increase the numerical accuracy and improve convergence.

5.3.2. QWs in the PDD solver

Quantum wells have been developed in the context of solar cells mainly to tailor the absorption edge of the subcells in a multi-junction devices to their optimum values [47]. Typically, achieving the proper performance requires a delicate trade-off between carrier collection and light absorption [48, 49]. Solcore includes a simplified QW structure in the PDD solver in order to calculate the performance of solar cells containing them. As pointed out, in Solcore's PDD solver, the structure of the energy levels available to the carriers is independent of the carrier density. This has important consequences in the presence of quantum wells in the structure. Solcore does not solve the Schrödinger equation and the PDD equations self-consistently: first, the energy levels of the quantum wells are solved using a flat-band condition and then an effective band structure is used to solve the transport equations in a bulk-like fashion. This is illustrated in Figure 11b.

From the perspective of the PDD solver, the actual bandgap and electron affinity of each layer in a quantum well depends on the energy levels, i.e. the minimum energy for electrons is not the band edge of the conduction band, but the ground confined level. The same applies to holes, being the actual band edge the maximum between the ground states of light holes and heavy holes.

To use QWs in the PDD solver, we create an effective electron affinity and band gaps for all layers in the QW. For the barriers, the electron affinity and band gap are the same than in bulk, modified by the strain, if necessary. For interlayers, if present, it depends on what is higher, the band edges of the interlayer or the confined carrier levels.

The density of states and the absorption profile need to be modified in a similar way. For the density of states:

- **Barriers** have the bulk density of states and absorption profile.
- **Interlayers** only have the bulk density of states above the barrier and the bulk absorption from the barrier energy and zero below that.
- **Wells** have all the density of states associated with the confined states and the bulk density of states above the barrier, while they have the absorption of the confined levels below the barrier energy and of the bulk above it.

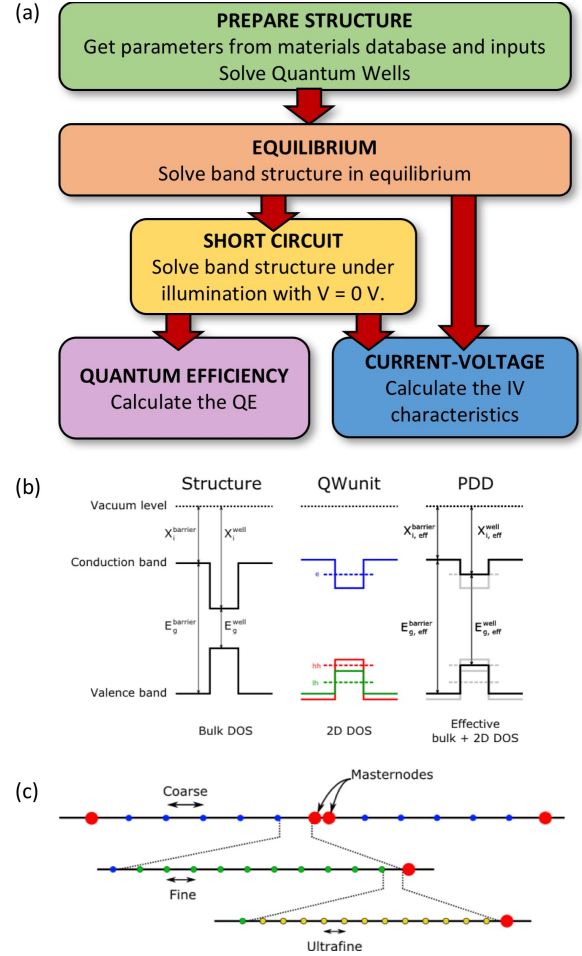


Figure 11: (a) Work flow of Solcore's PDD solver. (b) Process of obtaining the effective band structure of QWs to use in the PDD solver. From left to right: Simple sequence of layers. Band profile and energy levels after considering the strain and the quantum confinement. Effective band structure. (c) Description of the inhomogeneous mesh scheme used in Solcore.

These simplifications are similar to those in Nelson et al. [44] and in Cabrera et al. [50] and allow us to keep the bulk-like form of the carrier densities in the drift diffusion equations under the Boltzmann approximation.

5.3.3. Mesh creation and dynamic meshing

The PDD solver discretizes the device into a finite number of mesh points in which to calculate the band structure, carrier densities, the generation and recombination. The mesh can be static and homogeneous, but the default configuration and the one that results in the least number of mesh points, most accurate result and best convergence is by using an inhomogeneous mesh with dynamic re-meshing.

There are two types of nodes in the mesh: masternodes and normal nodes. There are two masternodes at the ends of the device and two more at each side of an interface separated by 0.1 nm. These nodes are static and not affected by re-meshing. The rest of the nodes are automatically distributed depending on the distance to the closest masternode, as illustrated in Figure 11c. During re-meshing, nodes can be added or removed according to the following rules:

An element will be divided into smaller elements by adding new nodes if any of the following statements is true:

- The variation of the potentials or the carrier densities across the element is big.
- The element is too close to the masternodes limiting the layer.
- The element is too big for the region.

A node will be removed if it fulfils all the following conditions:

- It is not a masternode.
- The variation of the potentials or the carrier densities with respect the previous and next nodes is small.
- It is not too close to the masternodes limiting the layer.
- If removing it does not create an element too big for the region.

After the initial meshing and every time there is a re-meshing, the position of the nodes (except that of the masternodes) is smoothed to avoid having adjacent elements too different in size. This re-meshing process is controlled by a *growth* parameter, which can be adjusted by the user.

Using the inhomogeneous mesh in addition to the dynamic re-meshing ensures that those regions where material properties change abruptly are modelled with more detail, aiding the convergence. It also allows to model devices including layers with very different thickness, such as QWs a few nanometers thick and bulk absorbers of several microns, without increasing significantly the number of nodes.

5.4. Depletion approximation

The depletion approximation is an analytical - or semi-analytical - solution to the Poisson-drift-diffusion equations described in the previous section applied to simple PN homojunction solar cells. It is based on the assumption that around the junction between the P and N regions, there are no free carriers and therefore all the electric field is due to the fixed, ionized dopants. This "depletion" of free carriers reaches certain depth towards the N and P sides; beyond this region, free and fixed carriers of opposite charges balanced and the regions are neutral. Under these conditions, the Poisson's equation decouples from the drift and diffusion equations and it can be solved analytically on each region. For example, for a PN junction with the interface between the two regions at $z = 0$, the solution to Eq. 43 will be:

$$\phi(z) = \begin{cases} 0 & \text{if } z < -w_p \\ \frac{qN_a}{2\epsilon_s}(z + w_p)^2 & \text{if } -w_p < z < 0 \\ -\frac{qN_d}{2\epsilon_s}(z - w_n)^2 + V_{bi} & \text{if } 0 < z < w_n \\ V_{bi} & \text{if } w_n < z \end{cases} \quad (53)$$

where w_n and w_p are the extensions of the depletion region towards the N and P sides, respectively, and can be found by the requirement that the electric field F and the potential ϕ need to be continuous at $z = 0$. V_{bi} is the built-in voltage, which can be expressed in terms of the doping concentration at each side, N_d and N_a , and the intrinsic carrier concentration in the material, n_i^2 :

$$V_{bi} = \frac{k_b T}{q} \ln \left(\frac{N_d N_a}{n_i^2} \right) \quad (54)$$

Another consequence of the depletion approximation is that the quasi-Fermi level energies are constant throughout the corresponding neutral regions and also constant in the depletion region, where their separation is equal to the external bias qV . Based on these assumptions, Eq. 44 and 45 simplify and analytical expressions can be found for the dependence of the recombination and generation currents as a function of the applied voltage. A full derivation of those expressions is included in Nelson [44].

Solcore's implementation of the depletion approximation includes two modifications to the basic equations. The first one is allowing for an intrinsic region to be included between the P and N regions to form a PiN junction. For low injection conditions (low illumination or low bias) this situation can be treated as described before, simply considering that the depletion region is now widened by the thickness of the intrinsic region. No low doping level is allowed for this region, at the moment.

In the equations provided by Nelson, the generation profile is given by the BL law (Eq. 18) which has an explicit dependence with z and results in analytic expressions for the current densities. In Solcore, we integrate the expressions for the drift-diffusion equations under the depletion approximation numerically to allow for an arbitrary generation profile calculated with any of the methods described in Section 4. It should be noted that although the equations are integrated numerically this will

not be a self-consistent solution of the Poisson-drift-diffusion equations, as it is done by the PDD solver (Section 5.3).

6. Multi-junction solar cells

A complete photovoltaic solar cell includes one or more junctions, metal contacts, optical layers (including anti-reflective coatings and nano-phonic structures) and tunnel junctions. The junctions, in turn, might range from simple PN homojunctions to complex heterojunctions, including multi-quantum well structures. The solvers described in Section 5 only calculate the properties of single junction devices. To combine them into a multi-junction device, it is necessary to consider that the individual junctions are electrically connected in series and the potential coupling of light emitted by the wider bandgap junctions into those with smaller bandgap.

6.1. No radiative coupling

We consider first the case of no radiative coupling between junctions. This is a good approximation for non-very radiative materials or radiative materials working at low concentration, when the fraction of radiative recombination compared to the non-radiative one is low. In this case, the IV curve of each junction can be calculated independently of each other and the current flowing through the MJ structure is limited by the junction with the lowest current at any given voltage. Series resistances defined for each junction are now added together and included as a single term. The operating voltage of each of the junctions is finally back calculated and added together to get the voltage of the MJ device.

The pseudocode for this solver is:

1. Calculate the $I_j(V)$ of each junction j in the structure.
2. Find the current flowing through the MJ device as $I_{MJ}(V) = I_j(V)$, if $|I_j(V)| = \min(|I_1(V)| \dots |I_N(V)|)$.
3. Calculate the voltage of each junction by interpolating their IV curve at the new current values, $V_j(I_{MJ})$, and the voltage dropped due to the series resistances, $V_{Rs} = R_s I_{MJ}$.
4. Calculate the total voltage at a given current as $V_{MJ} = V_{Rs} + \sum_j V_j$.
5. Interpolate the $I_{MJ}(V_{MJ})$ and the $I_{MJ}(V_j)$ to the desired output voltage values.

Fig. 12 shows the simulated IV curve of a 3J solar cell made of Ge/InGaAs/GaAsP. The three junctions were calculated using the depletion approximation solver. In the dark (Fig. 12a) the voltage of each of the junctions at a given current add together, resulting in the total voltage of the MJ structure. The R_s contribution to the voltage goes in the same direction that those of the junctions. Under illumination (Fig. 12b) the junction producing the lower current (the top junction in this case) limits the overall current of the MJ device. At zero, or even at some negative bias, the non-limiting junctions are positively biased, recombining all the photocurrent that cannot be extracted because of the limiting top cell. The contribution of the R_s to the voltage of the MJ device is negative, resulting in a reduction of the fill factor and the overall efficiency of the solar cell.

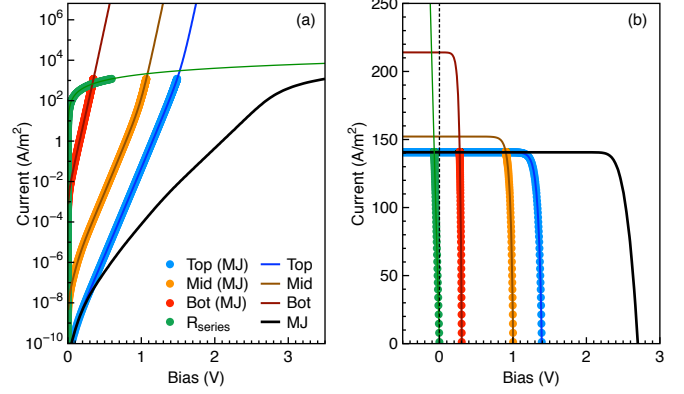


Figure 12: (a) Dark IV curve of a MJ solar cell, including the IV of the individual junctions separately (continuous lines) and the junctions as part of the MJ structure. (b) Light IV curve of the same MJ solar cell.

6.2. With radiative coupling

Radiative coupling takes place when the light produced by a high bandgap junction due to radiative recombination is absorbed by a lower bandgap junction, contributing to its photocurrent and changing the operating point. It has been identified in numerous highly radiative materials such as quantum well solar cells and III-V MJ solar cells [51, 52, 53]. It appears as an artefact during the QE measurements of MJ solar cells [54], but it is also an effect that can be exploited to increase the performance of MJ devices [47] and their tolerance to spectral changes, resulting in superior annual energy yield [55].

The radiative coupling formalism included in Solcore is based on the works by Chan et al. and Nelson et al. [55, 14]. It is implemented only for the DB junction model and for the 2D model when it is defined in terms of a radiative efficiency and the parameters calculated from the DB model. The current of a junction j including radiative coupling from the junction immediately above it $j-1$ is given by:

$$J_j^{total} = J_j^{nc} + J_{j-1 \rightarrow j}^{coupled} \quad (55)$$

This current depends on two factors: the amount of radiation effectively emitted downwards, towards the lower junction, and the fraction of it that is absorbed and converted into electricity. If we ignore the possible reflection of light at the interface between both junctions, this current can be written by using a modified version of Eq. 28 that considers only the radiation emitted towards the back:

$$J_{j-1 \rightarrow j}^{coupled}(V, T) = q \frac{2n^2}{h^3 c^2} \int_0^\infty \frac{E^2}{e^{\frac{E-qV}{k_b T}} - 1} A_{j-1 \rightarrow j}(E) dE \quad (56)$$

with $A_{j-1 \rightarrow j}(E)$ given by:

$$A_{j-1 \rightarrow j}(E) = 2\pi \int_0^1 \left[1 + r(E, \theta) e^{-\alpha_{j-1} w_{j-1} / \cos \theta} \right] \times \left(1 - e^{-\alpha_{j-1} w_{j-1} / \cos \theta} \right) \left(1 - e^{-\alpha_j w_j / \cos \theta} \right) \cos \theta d(\cos \theta) \quad (57)$$

As it was discussed before, any information related to total internal reflection will be contained in the $r(E, \theta)$ term, and therefore the integral on the $\cos \theta$ can be done from 0 to 1. In the case of thin junctions, some radiation could reach the next junction $j + 1$. The coupled current in that case can be easily calculated by modifying Eq. 57 to account for the fraction of light absorbed by the junctions between the emitting junction and the junction of interest. In the general case, the current coupled into junction j will be given by:

$$J_j^{\text{coupled}} = \sum_{i=1}^{j-1} J_{i \rightarrow j}^{\text{coupled}} \quad (58)$$

Radiative coupling might change the junction that is current limiting the MJ device, so the process to obtain the IV curves in this case proceeds in two steps. First, the IV of the junctions and the total IV are calculated without coupling. The resulting IV curves are then used as the initial conditions for the numerical solver that will calculate the correct voltage of each junction including the radiative coupling.

6.3. Restrictions in the Junction definitions

Having multiple methods for modelling the junctions gives a lot of freedom and flexibility but it also imposes some restrictions in how and when they can be combined in order to create a MJ solar cell. The following compatibility rules apply:

- When there is no radiative coupling and we are interested only in the dark IV characteristics, all junction models can be combined with each other. This allows to have a MJ device where the top junction is defined using the DB model, the middle one defined with the 2D model and the bottom one using a more accurate PDD model, for example.
- The same applies for light IV and quantum efficiency simulations as long as the optical model chosen is the BL law. In this case, any junction defined using the 2D model needs to include an absorptivity value.
- The TMM and RWCA optical models are supported only by the PDD and DA junction models.
- In the presence of radiative coupling, the only junction models that can be used are DB and 2D, as long as the later includes an absorptivity value.

6.4. Tunnel junctions

Solcore includes partial support for tunnel junctions. They represent an optical loss due to parasitic absorption in the layers, and an electrical loss modelled as a series resistance, which needs to be provided as input. This approximation should be valid in most cases, but it does not include the correct bias dependence of a tunnel junction and it will lead to the wrong results if the current is close to or higher than the peak current density of the junction.

7. Large circuit solver

The building blocks described in the previous sections to model single junctions and MJ solar cells can be combined to model larger circuits. Solcore includes two levels of large scale circuits: quasi-3D solar cell modelling and solar array modelling. Both solvers are based on the interface between Solcore and SPICE, allowing for a fast calculation of complex structures with many elements.

7.1. Quasi-3D solar cell model

The quasi-3D solar cell model included in Solcore is based on a SPICE-based electrical network to model the flow of injected current through the solar cell, as depicted in Fig. 13. The plane of the cell is discretized into many elements, each of them representing a small portion of the cell. Depending on the location of the element - exposed to the sunlight or underneath a metal finger - the IV curve of the cell will be the light IV or the dark IV. Each element is linked to their neighbours with resistors, representing the lateral current flow and dependent on the sheet resistance of the cells. This method can be applied to any number of junctions.

This type of formalism is widely used to simulate the performance of solar cells when the effect of a spatial variable need to be incorporated in the model. Such variable can be the design of the front metal grid, in order to minimise the effect of series resistances [Steiner 2010], the inhomogeneous illumination profile in concentrator devices and the impact of such inhomogeneity into the transport through the tunnel junctions [56, 57], or the distribution of defects or inhomogeneities [58, 59]. More recently, we used this formalism to model the photoluminescence and the electroluminescence based IV curves of MJ devices, accounting for the limited lateral carrier transport [60].

7.1.1. In-plane discretization

As shown in Fig. 13, there are two regions in the plane: the metal and the aperture. These two are provided to Solcore as grey scale images that will work as masks. The resolution of the images, in pixels, will define the in-plane discretization. By default, the aspect ratio of the pixels in the image will be 1:1, but this can be set to a different value in order to reduce the number of elements and improve speed. For example, the in-plane discretization of Fig. 13a, has an aspect ratio $A_r = L_y/L_x = 4$, with L_x and L_y the pixel size in each direction. The values of the pixels in the metal mask are 0 where there is no metal (the aperture area), 255 where there is metal and the external electrical contacts (the boundaries with fixed, externally set voltage values) and any other value in between to represent regions with metal but not fixed voltage. The pixels of the illumination mask - which become the aperture mask after removing the areas shadowed by the metal - can have any value between 0 and 255. These values divided by 255 will indicate the intensity of the sunlight at that pixel relative to the maximum intensity. Fig. 14 illustrates two examples of metal mask (a) and (b) and an illumination mask (c) with 120×120 pixels. As it can be seen, while rectangular metal fingers are well reproduced, diagonal fingers are less accurate and could require a finer discretization.

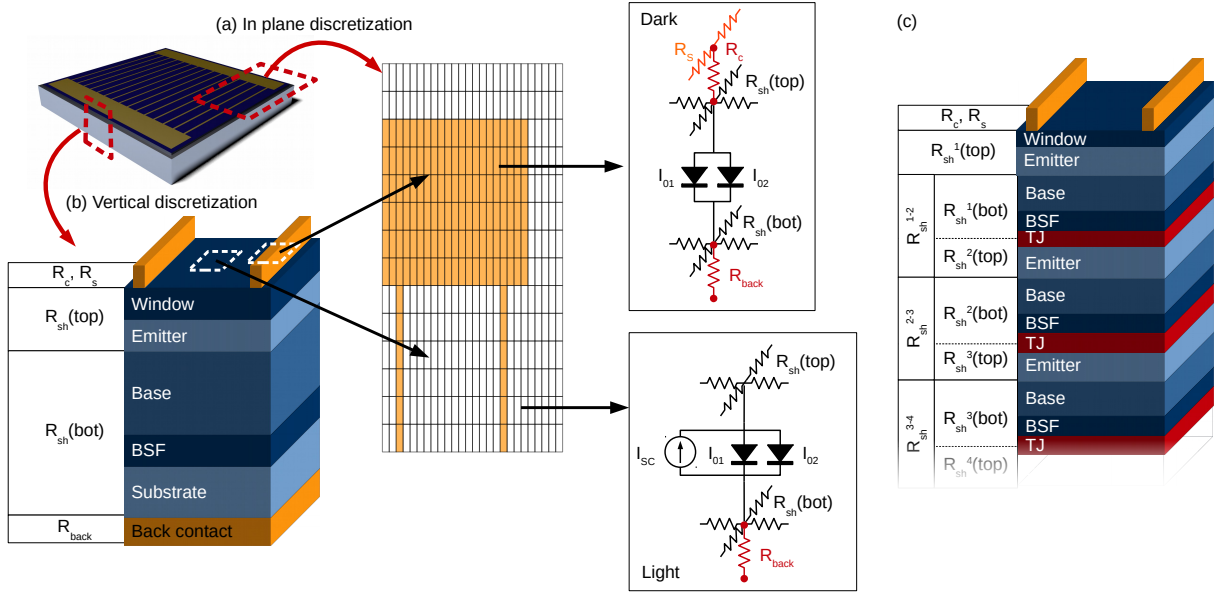


Figure 13: Schema of the quasi-3D solar cell modelling included in Solcore. The solar cell is discretized (a) in the plane and (b) in the vertical direction. Illuminated and dark regions are then modelled using electrical components that, when combined, form a 3D electrical mesh giving the voltages and currents at any point of the structure. (c) An example of the vertical discretization of a N-junction solar cell.

The illumination mask is mostly homogeneous except around the edges and in the corners, where intensity is much lower. This pattern could be produced, for example, the secondary optics of a concentration system.

In the simplest case, this scheme requires that the individual junction IV curves be solved in just two situations: in the dark and under illumination, which will be used for the metal pixels and the aperture pixels respectively. In the most complex scenario, the aperture mask will have the whole range of light intensities, from 0 to 255, meaning that the IV curves will need to be calculated in 256 situations. Often, it will not be necessary to have 256 illumination levels and 8 or 10 will suffice to produce accurate results, even when simulating very inhomogeneous illumination.

The minimum total number of nodes where SPICE will need to calculate the voltages will be $N \times M \times Q$, with N and M the number of pixels in both in-plane directions and Q the number of junctions. To this, the front and back metal contacts could add a maximum of $2M \times M$ nodes. Exploiting symmetries of the problem as well as choosing an appropriate pixel aspect ratio will significantly reduce the number of nodes and therefore the time required for the computation of the problem.

7.1.2. Vertical discretization

The IV curve of each junction in the solar cell is calculated as described in Section 5 and 6. The individual IV curves are then incorporated into SPICE as voltage dependent current sources. The solar cell needs to be solved for each of the illumination levels, as described in the previous section. This process can be simplified for junctions using the DB, 2D and DA models as the photocurrent and the recombination currents are independent,

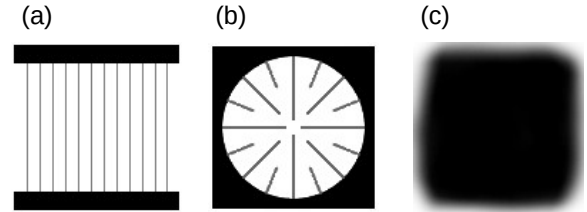


Figure 14: (a) and (b) two examples of metal masks and (c) an illumination mask. The thin metal fingers in (a) and (b) are grey, indicating that there is metal in those pixels but that their bias is not set to be equal to the external bias.

but that is not the case for the PDD junction model, especially under concentration.

Sheet resistances above and below each junction, $R_{sh}(top)$ and $R_{sh}(bot)$, account for the lateral transport. Beneath the metal, there is no current source, as the region is in the dark, and there are extra resistances accounting for the contact between the metal and the semiconductor R_c and the transport along the metal finger R_s [Steiner 2010]. Given that the pixels can be asymmetric, these resistances need to be defined in both in-plane directions, x and y :

$$R_{sh}^x = \frac{1}{A_r} R_{sh} \quad (59)$$

$$R_{sh}^y = A_r R_{sh} \quad (60)$$

$$R_s^x = \frac{1}{h A_r} \rho_m \quad (61)$$

$$R_s^y = \frac{A_r}{h} \rho_m \quad (62)$$

$$R_c = R_{back} = \frac{1}{L_x^2 A_r} \rho_c \quad (63)$$

where h is the height of the metal, ρ_m their linear resistivity and ρ_c the contact resistivity between metal and semiconductor. The sheet resistance of a stack of semiconductor layers R_{sh} is equal to the combination in parallel of the individual sheet resistances. Using the single junction example of Fig. 13, $R_{sh}(top)$ will be given by:

$$\frac{1}{R_{sh}(top)} = \frac{1}{R_{sh}(window)} + \frac{1}{R_{sh}(emitter)} \quad (64)$$

Each of these can be estimated from the thickness of the layer d , the majority carrier mobility μ and the doping N as [Steiner 2011]:

$$\frac{1}{R_{sh}} = qd\mu N \quad (65)$$

If the solar cell has been defined using only the DA and PDD junction models, this information is already available for all the layers of the structure. For junctions using the DB and 2D models, R_{sh} will need to be provided for the top and bottom regions of each junction. Intrinsic layers will be ignored as they do not contribute to the lateral current transport.

7.2. Solar array model

The ability to link use solCore to build a SPICE equivalent circuit enables entire PV systems to be simulated from the bottom up [61]. Each photovoltaic solar cell is described using an equivalent circuit which can then be arranged in strings of series and parallel to represent the entire system. An example of a triple junction solar cell, complete with a bypass diode is shown in figure 15; this unit is the basic building block for a concentrator PV module [41].

The diode and resistance values for the equivalent circuit are determined from solar cell testing, while the current source is evaluated by integrating the product of the spectral irradiance (estimated using an appropriate radiative transfer code e.g. SPCTRL2 or SMARTS) and the quantum efficiency which in turn can be calculated dynamically as a function of temperature by Solcore [62].

Since the entire module (and subsequently the system) is assembled from individual solar cell components, it is possible and indeed, necessary to distribute the component values to accommodate for manufacturing tolerances. This enables a close match between the modelled output power and that measured experimentally and has been used to determine how both aerosols and precipitable water affect the electricity yield from

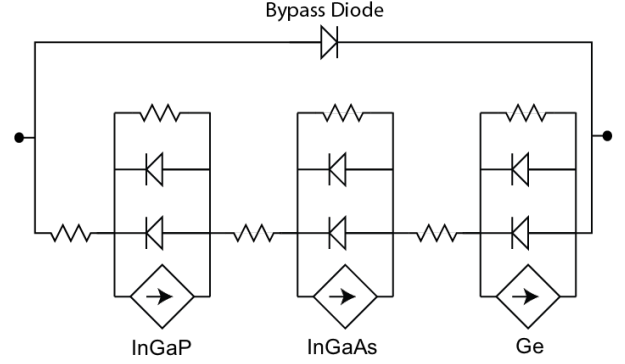


Figure 15: Equivalent circuit for a triple junction solar cell

concentrator PV systems [63, 64]. Where system IV data is available, the emergence of electrical faults, e.g. shunts or shading can also be accounted for [65].

8. Closing remarks

In conclusion, along this article we have described the capabilities of Solcore, a multi-scale, python-based, modular simulation framework of semiconductor materials and solar cells. Its main strengths are:

- **Flexibility:** Provides a variety of tools, rather than a single solution, for the study of traditional and novel semiconductor materials and devices.
- **Modularity:** Can be expanded with new capabilities, innovative solvers and tools.
- **Accessibility:** Not only it is open source, but also it is designed to be easy to learn and to use, serving as teaching tool as much as research tool.
- **Rigour:** The physics behind every functionality are well understood and supported by numerous references, as well as the approximations made in order to simplify the implementation of the problem or the interpretation of the results.
- **Integrated:** All of Solcore's functionality are designed to be compatible with each other to allow for a truly multi-scale modelling in an integrated way.

Acknowledgements

Solcore is not the creation of a single person but the combined effort of present and past members of the Quantum Photovoltaics Group at Imperial College London. Therefore, the authors would like to thank to all those people that contributed to its development: M. Führer, D. Farrel, T. Thomas and N. L. A. Chan.

References

References

- [1] C. Gueymard, SMARTS2 (1995).
- [2] J. Eisenlohr, N. Tucher, O. Höhn, H. Hauser, M. Peters, P. Kiefel, J. C. Goldschmidt, B. Bläsi, Matrix formalism for light propagation and absorption in thick textured optical sheets, *Optics Express* 23 (11) (2015) A502.
- [3] S. C. Baker-Finch, K. R. McIntosh, A freeware program for precise optical analysis of the front surface of a solar cell, in: 2014 IEEE 40th Photovoltaic Specialist Conference (PVSC), IEEE, 2010, pp. 002184–002187.
- [4] A. Fell, A Free and Fast Three-Dimensional/Two-Dimensional Solar Cell Simulator Featuring Conductive Boundary and Quasi-Neutrality Approximations, *IEEE Transactions on Electron Devices* 60 (2) (2013) 733–738.
- [5] R. Varache, C. Leendertz, M. Gueunier-Farret, J. Haschke, D. Muñoz, L. Korte, Investigation of selective junctions using a newly developed tunnel current model for solar cell applications, *Solar Energy Materials and Solar Cells* 141 (Supplement C) (2015) 14–23.
- [6] S. Birner, T. Zibold, T. Andlauer, T. Kubis, M. Sabathil, A. Trellakis, P. Vogl, nextnano: General Purpose 3-D Simulations, *IEEE Transactions on Electron Devices* 54 (9) (2007) 2137–2142.
- [7] Silvaco, Atlas: Device Simulation Framework.
- [8] R. W. Andrews, J. S. Stein, C. Hansen, Introduction to the open source PV LIB for python Photovoltaic system modelling package, 2016 IEEE 43rd Photovoltaic Specialists Conference (PVSC) (2014) 0170–0174.
- [9] I. Vurgaftman, J. R. Meyer, L. R. Ram-Mohan, Band parameters for III–V compound semiconductors and their alloys, *Journal of Applied Physics* 89 (11) (2001) 5815–61.
- [10] M. Levinshtein, S. Rumyantsev, M. Shur, M. Levinshtein, S. Rumyantsev, M. Shur, Handbook Series on Semiconductor Parameters, Vol. 2 of Volume 2: Ternary And Quaternary III-V Compounds, WORLD SCIENTIFIC, 2012.
- [11] M. Sotoodeh, A. H. Khalid, A. A. Rezazadeh, Empirical low-field mobility model for III–V compounds applicable in device simulation codes, *Journal of Applied Physics* 87 (6) (2000) 2890–12.
- [12] Software Spectra Inc., Optical Data from Sopra S. A. (2008).
- [13] M. Paxman, J. Nelson, B. Braun, J. CONNOLLY, K. W. J. Barnham, C. T. Foxon, J. S. Roberts, Modeling the spectral response of the quantum well solar cell, *Journal of Applied Physics* 74 (1) (1993) 614–621.
- [14] J. Nelson, J. Barnes, N. Ekins-Daukes, B. Klufinger, E. Tsui, K. Barnham, C. T. Foxon, T. Cheng, J. S. Roberts, Observation of suppressed radiative recombination in single quantum well p-i-n photodiodes, *Journal of Applied Physics* 82 (12) (1997) 6240–6246.
- [15] J. Nelson, I. Ballard, K. Barnham, J. P. Connolly, J. S. Roberts, M. Pate, Effect of quantum well location on single quantum well p-i-n photodiode dark currents, *Journal of Applied Physics* 86 (10) (1999) 5898–9.
- [16] M. F. Fuhrer, J. G. J. Adams, K. W. J. Barnham, B. C. Browne, N. L. A. Chan, D. J. Farrell, L. Hirst, K.-H. Lee, N. J. Ekins-Daukes, A. Ogura, K. Yoshida, Y. Okada, Extensible modelling framework for nanostructured III-V solar cells, 2011 37th IEEE Photovoltaic Specialists Conference (PVSC) (2011) 002615–002618.
- [17] M. Führer, D. Farrell, N. Ekins-Daukes, CPV modelling with Solcore: An extensible modelling framework for the rapid computational simulation and evaluation of solar cell designs and concepts, in: 9th International Conference on Concentrator Photovoltaic Systems: CPV-9, AIP, 2014, pp. 34–37.
- [18] S. Tomic, Electronic structure of InyGa1-yAs1-xNx/GaAs(N) quantum dots by ten-band kpt theory, *Physical Review B* 73 (12) (2006) 125348–8.
- [19] M. Volk, S. Lutgen, T. Marschner, W. Stolz, E. O. Göbel, P. C. M. Christianen, J. C. Maan, Carrier effective masses in symmetrically strained (GaIn)As/Ga(PAs) multiple-quantum-well structures, *Physical Review B* 52 (15) (1995) 11096–11104.
- [20] W. R. Frensley, Numerical evaluation of resonant states, Superlattices and Microstructures 11 (3) (1992) 347–350.
- [21] S. Adachi, Model dielectric constants of GaP, GaAs, GaSb, InP, InAs, and InSb, *Physical Review B* 35 (14) (1987) 7454–7463.
- [22] S. Adachi, Optical dispersion relations for GaP, GaAs, GaSb, InP, InAs, InSb, Al_xGa_{1-x}As, and In_{1-x}Ga_xAs_yP_{1-y}, *Journal of Applied Physics* 66 (12) (1989) 6030–6040.
- [23] S. Adachi, Optical dispersion relations for Si and Ge, *Journal of Applied Physics* 66 (7) (1989) 3224–3231.
- [24] A. D. Rakić, M. L. Majewski, Modeling the optical dielectric function of GaAs and AlAs: Extension of Adachi's model, *Journal of Applied Physics* 80 (10) (1996) 5909–5914.
- [25] C. C. Kim, J. W. Garland, H. Abad, P. M. Raccach, Modeling the optical dielectric function of semiconductors: Extension of the critical-point parabolic-band approximation, *Physical Review B* 45 (20) (1992) 11749–11767.
- [26] C. C. Kim, J. W. Garland, P. M. Raccach, Modeling the optical dielectric function of the alloy system Al_xGa_{1-x}As, *Physical Review B* 47 (4) (1993) 1876–1888.
- [27] J. A. Woollam, Guide to Using WVASE32, J. A. Woollam Co. Inc. (2012).
- [28] E. D. Palik, Gallium Arsenide (GaAs), in: Handbook of Optical Constants of Solids, Elsevier, 1997, pp. 429–443.
- [29] T. Wilson, A. Mellor, N. P. Hylton, N. J. Ekins-Daukes, The Effects of Short-Range Alloy Disorder on the Potential Voltage Performance in GaAsBi Based Solar Cells, In Preparation.
- [30] P. C. Klipstein, N. Apsley, A theory for the electroluminescence spectra of quantum well structures, *Journal of Physics C: Solid State Physics* 19 (32) (2000) 6461–6478.
- [31] S. L. Chuang, Physics of Optoelectronic Devices, Wiley-Interscience, 1995.
- [32] R. Galleano, W. Zaiman, D. Alonso-Álvarez, A. Minuto, N. Ferretti, R. Fucci, M. Pravettoni, M. Halwachs, M. Friederichs, F. Plag, D. Friedrich, E. Haverkamp, Results of the Fifth International Spectroradiometer Comparison for Improved Solar Spectral Irradiance Measurements and Related Impact on Reference Solar Cell Calibration, *IEEE Journal of Photovoltaics* 6 (6) (2016) 1587–1597.
- [33] T. Wilson, T. Thomas, M. Führer, N. J. Ekins-Daukes, Addressing reflectivity losses in multi-junction solar cells to achieve 50% conversion efficiency, *Materials Research Innovations* 19 (7) (2016) 503–507.
- [34] D. Alonso-Álvarez, L. Ferre Llin, A. Mellor, D. J. Paul, N. J. Ekins-Daukes, ITO and AZO films for low emissivity coatings in hybrid photovoltaic-thermal applications, *Solar Energy* 155 (2017) 82–92.
- [35] H. A. Macleod, Thin-film optical filters, Institute of Physics Publishing, Bristol and Philadelphia (2001).
- [36] S. J. Byrnes, Multilayer optical calculations, [arXiv.org arXiv:1603.02720v2](https://arxiv.org/abs/1603.02720v2).
- [37] V. Liu, S. Fan, S4: A free electromagnetic solver for layered periodic structures, *Computer Physics Communications* 183 (10) (2012) 2233–2244.
- [38] A. Martí, G. L. Araújo, Limiting efficiencies for photovoltaic energy conversion in multigap systems, *Solar Energy Materials and Solar Cells* 43 (2) (1996) 203–222.
- [39] N. L. A. Chan, N. J. Ekins-Daukes, J. G. J. Adams, M. P. Lumb, M. Gonzalez, P. P. Jenkins, I. Vurgaftman, J. R. Meyer, R. J. Walters, Optimal Bandgap Combinations - Does Material Quality Matter?, *IEEE Journal of Photovoltaics* 2 (2) (2012) 202–208.
- [40] T. Thomas, A. Mellor, N. P. Hylton, M. Führer, D. Alonso-Álvarez, A. Braun, N. J. Ekins-Daukes, J. P. R. David, S. J. Sweeney, Requirements for a GaAsBi 1 eV sub-cell in a GaAs-based multi-junction solar cell, *Semiconductor Science and Technology* 30 (9) (2015) 094010.
- [41] N. J. Ekins-Daukes, Y. Kemmoku, K. Araki, T. R. Betts, R. Gottschalg, D. G. Infield, M. Yamaguchi, The design specification for Syracuse; A multi-junction concentrator system computer model, in: Proc. 19th European Photovoltaic Solar Energy Conference, 2004.
- [42] P. A. Basore, PC-1D version 3: improved speed and convergence, *IEEE 20nd Photovoltaic Specialists Conference* (1991) 299–302.
- [43] S. M. Sze, Physics of semiconductor devices; 2nd ed., Wiley, New York, NY, 1981.
- [44] J. Nelson, The physics of solar cells, London : Imperial College Press ; River Edge, NJ : Distributed by World Scientific Pub. Co, 2003.
- [45] P. A. Basore, PC-1D Installation Manual and User's Guide Version 3.1 (2009) 1–96.
- [46] P. A. Farrell, E. C. Gartland, On the Sharfetter-Gummer discretization for drift-diffusion continuity equations, in: J. J. H. Miller (Ed.), Computational methods for boundary and interior layers in several dimensions, 1991, pp. 51–79.
- [47] T. Thomas, T. Wilson, M. Führer, D. Alonso-Álvarez, N. J. Ekins-Daukes, D. Lackner, P. Kailuweit, S. P. Philipps, A. W. Bett, K. Toprasertpong, M. Sugiyama, Y. Okada, Potential for reaching 50% power conversion efficiency using quantum heterostructures, in: 6th World Conference on

- Photovoltaic Energy Conversion, 2014, pp. 1–2.
- [48] D. Alonso-Alvarez, M. Führer, T. Thomas, N. Ekins-Daukes, Elements of modelling and design of multi-quantum well solar cells, 2014 IEEE 40th Photovoltaic Specialists Conference (PVSC) (2014) 2865–2870.
 - [49] D. Alonso-Alvarez, N. J. Ekins-Daukes, Quantum wells for high-efficiency photovoltaics, in: A. Freundlich, L. Lombez, M. Sugiyama (Eds.), SPIE OPTO, SPIE, 2016, pp. 974311–12.
 - [50] C. I. Cabrera, J. C. Rimada, J. P. Connolly, L. HERNANDEZ, Modelling of GaAsP/InGaAs/GaAs strain-balanced multiple-quantum well solar cells, *Journal of Applied Physics* 113 (2) (2013) 024512–8.
 - [51] K.-H. Lee, K. W. J. Barnham, J. P. Connolly, B. C. Browne, R. J. Airey, J. S. Roberts, M. Führer, T. N. D. Tibbits, N. J. Ekins-Daukes, Demonstration of Photon Coupling in Dual Multiple-Quantum-Well Solar Cells, *IEEE Journal of Photovoltaics* 2 (1) (2012) 68–74.
 - [52] M. A. Steiner, J. F. Geisz, T. E. Moriarty, R. M. France, W. E. McMahon, J. M. Olson, S. R. Kurtz, D. J. Friedman, Measuring IV Curves and Subcell Photocurrents in the Presence of Luminescent Coupling, *IEEE Journal of Photovoltaics* 3 (2) (2013) 879–887.
 - [53] M. A. Steiner, J. F. Geisz, Non-linear luminescent coupling in series-connected multijunction solar cells, *Applied Physics Letters* 100 (25) (2012) 251106–6.
 - [54] M. A. Steiner, S. R. Kurtz, J. F. Geisz, W. E. McMahon, J. M. Olson, Using Phase Effects to Understand Measurements of the Quantum Efficiency and Related Luminescent Coupling in a Multijunction Solar Cell, *IEEE Journal of Photovoltaics* 2 (4) (2012) 424–433.
 - [55] N. L. A. Chan, T. Thomas, M. Führer, N. J. Ekins-Daukes, Practical Limits of Multijunction Solar Cell Performance Enhancement From Radiative Coupling Considering Realistic Spectral Conditions, *IEEE Journal of Photovoltaics* 4 (5) (2014) 1306–1313.
 - [56] K. Nishioka, T. Takamoto, T. Agui, M. Kaneiwa, Y. Uraoka, T. Fuyuki, Evaluation of InGaP/InGaAs/Ge Triple-Junction Solar Cell under Concentrated Light by Simulation Program with Integrated Circuit Emphasis, *Japanese Journal of Applied Physics* 43 (3) (2004) 882–889.
 - [57] M. Steiner, W. Guter, G. Peharz, S. P. Philipps, F. Dimroth, A. W. Bett, A validated SPICE network simulation study on improving tunnel diodes by introducing lateral conduction layers, *Progress in Photovoltaics: Research and Applications* 20 (3) (2011) 274–283.
 - [58] T. Jürgens, L. Gütay, G. H. Bauer, Photoluminescence, open circuit voltage, and photocurrents in Cu(In,Ga)Se₂ solar cells with lateral submicron resolution, *Thin Solid Films* 511–512 (2006) 678–683.
 - [59] M. Paire, L. Lombez, J.-F. Guillemoles, D. Lincot, Measuring sheet resistance of CIGS solar cell’s window layer by spatially resolved electroluminescence imaging, *Thin Solid Films* 519 (21) (2011) 7493–7496.
 - [60] D. Alonso-Álvarez, Imperial College London, London, United Kingdom, N. Ekins-Daukes, SPICE Modelling of Photoluminescence and Electroluminescence Based Current-Voltage Curves of Solar Cells for Concentration Applications, *Journal of Green Engineering* 5 (4) (2016) 33–48.
 - [61] L. Castaner, S. Silvestre, *Modelling PV-systems using PSPice*, Wiley, 2002.
 - [62] N. J. Ekins-Daukes, T. R. Betts, Y. Kemmoku, K. Araki, H. S. Lee, R. Gottschalg, M. B. Boreland, D. G. Infield, M. Yamaguchi, Syracuse - a multi-junction concentrator system computer model, in: *Proc. 31st IEEE Photovoltaic Specialists Conference*, 2005.
 - [63] N. L. A. Chan, T. B. Young, H. E. Brindley, N. J. Ekins-Daukes, K. Araki, Y. Kemmoku, M. Yamaguchi, Validation of energy prediction method for a concentrator photovoltaic module in Toyohashi Japan, *Progress in Photovoltaics Research and Applications*.
 - [64] N. L. A. Chan, H. E. Brindley, N. J. Ekins-Daukes, Impact of individual atmospheric parameters on CPV system power, energy yield and cost of energy, *Progress in Photovoltaics Research and Applications*.
 - [65] N. E.-D. Harsh G. Kamatha, K. Araki, S. K. Ramaseshaa, Performance analysis and fault detection method for concentrator photovoltaic modules, In preparation.